Test Plan

OWC-WEC with Deep Water Reactance

Awardee: HiSeas Energy, Inc.
Awardee Point of Contact: William Alexander
Test Facility: Texas A&M Offshore Technology Research Center
Test Facility Point of Contact: Richard Mercier
Numerical Modeling Facility: Sandia National Laboratories
Numerical Modeling Facility Point of Contact: Dominic Forbush

Date: 12/31/2021

Proprietary Information

Each Party agrees to not disclose Proprietary Information provided by another Party to anyone other than the CRADA Participant, Contractors, and their respective subcontractors (if any) performing work under this CRADA without written approval of the providing Party, except to Government employees who are subject to the statutory provisions against disclosure of confidential information set forth in the Trade Secrets Act (18 U.S.C. 1905). Government employees shall not be required to sign non-disclosure agreements due to the provisions of the above-cited statute. If Proprietary Information is orally disclosed to a Party, it shall be identified as such, orally, at the time of disclosure and confirmed in a written summary thereof, appropriately marked by the disclosing Party, within thirty (30) days as being Proprietary Information. All Proprietary Information shall be protected by the recipient for a period of five (5) years from the effective date of this CRADA, unless such Proprietary Information becomes publicly known without the fault of the recipient, shall come into recipient's possession without breach by the recipient of any of the obligations set forth herein, can be demonstrated by the recipient by written record that it is known prior to receipt from disclosing party, is disclosed by operation of law, or is independently developed by recipient's employees who did not have access to such Proprietary Information. Upon request, Proprietary Information in tangible form shall be returned to the disclosing Party at the disclosing Party's expense or destroyed with a certificate of destruction submitted to the disclosing Party upon termination or expiration of this CRADA, or during the term of this CRADA upon request by the disclosing Party, except that the receiving Party may keep an archival copy of the Proprietary Information for the sole purpose of verifying the receiving Party's compliance with this Agreement

Executive Summary

From September 20 to October 12, 2021 physical model tests of the HiSeas OWC-WEC were conducted at the Offshore Technology Research Center (OTRC) in College Station, Texas. The goal of the model test program was to measure the performance of the WEC in a range of regular and irregular wave conditions so that the data could be used for validating a numerical model of the WEC hydro-mechanics. The tests were conducted at a scale of 1:35 and Froude scaling was applied. The measurements included oscillating water column elevation, air pressure in the oscillating water column chamber, WEC motions, and mooring tension. The physical model of the WEC was provided to the OTRC by HiSeas Energy.

A WEC-Sim model of the oscillating water column device was constructed using boundary element method code WAMIT and mass/inertia estimates provided by HiSeas. Two versions of the WEC-Sim model were constructed: one with a simplified spring-damper PTO capable of delivering reactive power, and a second modeling a passive orifice to be tuned to experimental results described above. The results of the modeling demonstrate that while controllers with reactive power can significantly increase mechanical power capture, the PTO must be carefully co-designed to ensure that this benefit is economically translated to electrical power capture. In the orifice model, the drag coefficients in heave, surge, and pitch were adjusted along with the effective orifice diameter to match observed dynamics in free-decay tests. The most impactful tuning parameter was effective orifice diameter, implying that viscous effects of the oscillating flows were significant. The model matches power well except in regular waves near resonance and at low frequencies in irregular seas, both of which suggest limitations in the accuracy of the boundary element method code.

1 Introduction to the project

HiSeas Energy is developing a new kind of Wave Energy Converter (WEC) to supply low cost renewable energy from the oceans. The HiSeas WEC is a unique variation on the conventional Spar Buoy Oscillating Water Column (OWC) WEC. The HiSeas WEC uses a large volume of entrained sea water in a spherical "Stabilizer" at the bottom of a 100 meter long steel tube (spar), which connects the Stabilizer to an open bottom, closed top, thin-walled cylinder which forms the OWC. The Stabilizer provides the reaction mass needed to extract energy from wave motion yet allows the cylinder to freely move laterally in response to surge, with minimal side loads on the cylinder or bending moments in the spar. Simulations and structural analysis indicate that each device of this type may generate up to 1 MW of power from a top-mounted bi-directional turbine, such as the Siemens HydroAir Turbine, with a mass per unit of power of 93 tons per MW.

The Device Under Test (DUT) is shown below in Figure 1.

Figure 1: Photograph of experimental model.

This project will test a working model in Texas A&M's OTRC Wave Basin as well as perform numerical modeling at Sandia National Laboratories (SNL). The former will serve to calibrate and validate the latter. The overall objective of this work is to provide accurate predictions of the power output of this device in various sea states. That, combined with structural analysis and resulting mass estimates, will be used to predict power to weight ratio, capacity factor, and LCOE of the full scale device.

Testing at OTRC will largely consist of subjecting the DUT to various regular, irregular, and white noise wave conditions while monitoring and recording its 6DOF motion, OWC pressure and fluctuating water level.

Numerical modeling at SNL will develop a Boundary Element Method model of the WEC which will advise the test matrix, including 1-DOF and 3/6-DOF models with an idealized orifice. The simulations will be tuned to match test basin results. If necessary, the complexity of the 3/6DOF model will be increased to include additional internal free-surface dynamics (assuming internal water height measurements are available). The WEC-Sim models will be enhanced with realistic PTO model(s) and controllers.

2 Roles and Responsibilities of Project Participants

2.1 Applicant Responsibilities and Tasks Performed

The Applicant, HiSeas Energy, is responsible for the DUT, the Test Plan, Test Report, and technical coordination between HiSeas Energy, OTRC, and SNL. Tasks to be performed are:

1. Work with OTRC and SNL to complete and submit the Test Plan, which includes a Statement of Work (SOW) for SNL.
2. Determine certain mass properties of the DUT (Stabilizer volume, total dry mass).
3. Deliver the DUT to OTRC prior to testing.
4. Work with OTRC on any issues arising during wave basin tests.
5. Retrieve the DUT after testing is complete.
6. Work with SNL on any issues arising during their Numerical Modeling.

7. Work with OTRC and SNL to complete and submit the Post Access Report.

2.2 Network Facility Responsibilities and Tasks Performed

The Offshore Technology Research Center is responsible for testing the DUT as well as recording the test data. Tasks to be performed are:

1. Work with HiSeas Energy and SNL to complete and submit the Test Plan.
2. Execute the Test Plan.
3. Deliver the test data and analysis results to HiSeas Energy and SNL.

Sandia National Laboratories is responsible for the numerical analysis. Tasks to be performed are:

1. Develop boundary-element-method model of OWC with deep-water reactance. This will lead to a low-order linear model, which will advise experimental test matrix.
2. Build 1-DOF and simple 3/6-DOF model of OWC with idealized orifice in WEC-Sim to replicate laboratory experiments.
3. Tune simulation based on laboratory results.
4. If necessary: increase complexity of 3/6DOF model to include additional internal free-surface dynamics (assuming internal water height measurements are available).
5. Enhance appropriate WEC-Sim model with realistic PTO model(s) and controllers.
6. Perform model design iterations/optimizations as directed and available.

It should be noted that due to testing delays, step 3) and step 4) were actually completed last chronologically.

3 Project Objectives

The main objective is to numerically model this device at both model and full scale and to use wave basin testing to validate the model.

The 1:35 scale test model will be large enough to require wave lengths and periods within the range of the wave basin, while being within the depth capabilities of the basin. Basin testing will have the primary objective of recording chamber pressure, chamber oscillating water level, and spar motion over a wide range of wave height and periods, corresponding to the full range of open sea conditions at scale. Two variations on the orifice diameter will provide additional data for verification of the simulations.

Numerical modeling will simulate the 6-DOF motion of the device in a wide range of sea states and predict the resulting chamber pressures while simulating the operation of bi-directional air turbine such as the Siemens HydroAir Turbine. This will give greater confidence in predictions of full scale performance, which will facilitate predictions of output power and LCOE after capacity factor and structural analysis have been done.

This project has no specifically targeted performance metrics. The intent of the project is to characterize this WEC technology for power production and cost of power production. However, this technology was conceived with the intent to produce a WEC with competitive performance metrics, including power to weight and LCOE. This project will provide guidance on computing those metrics.

4 Test Facility, Equipment, Software, and Technical Expertise

The wave basin testing will be done at Texas A&M's Offshore Technology Research Center under the direction of Dr. Richard Mercier. The OTRC is well suited due to its deep basin. As the model has about a 3 meter draft, the wave basin should be at least twice that depth to simulate the deep ocean. The OTRC has a 5.8 meter depth and can easily generate the full spectrum of regular and irregular waves needed for testing. The OTRC has optical equipment for tracking device motion, and will also provide the pressure sensors to track the chamber pressure within the cylinder. This pressure, and the orifice diameter, relate to power generation (power generation = turbine efficiency $\times$ volume flow rate $\times$ pressure drop - for

incompressible flow). The OTRC will also provide two water elevation sensors to measure the fluctuations of the oscillating water column and an in-line load cell to measure the tension at the attachment of the mooring line to the WEC.

Numerical Modeling at Sandia National Laboratories will be led by Dr. Dominic Forbush. Given a device geometry, this will employ boundary element methods (BEM) and the Wave Energy Converter Simulator (WEC-Sim) to develop frequency and time domain models (respectively) of the device in question. Initial modeling efforts will aim to replicate the basin testing data to the extent possible, tuning the models, which can then be used for subsequent investigation of device improvement approaches, power-take-off design, and control strategies. Sandia National Laboratories, together with the National Renewable Energy Laboratory, has developed and utilized the WEC-Sim software package since its inception in 2014, and has conducted numerous studies in WEC-Sim involving novel WEC archetypes and controls investigations. A low-to-medium fidelity model, WEC-Sim is well-suited to the early-stage investigation of WEC technologies. Implemented in MATLAB Simulink, a broad suite of controller development and power-take-off simulation tools are also available.

5 Test or Analysis Article Description

The Oscillating Water Column WEC with Deep Water Reactance consists of a large hollow sphere ("Stabilizer") which is filled with seawater, a hollow cylinder at the top of the device, with the cylinder having a bottom open to the sea and a sealed top save for an orifice which leads to an air turbine, and a long, narrow rod (spar) connecting the Stabilizer with the cylinder. A small amount of ballast at the bottom of the spar, and a small amount of floatation in the cylinder keep the device upright in the sea. The flotation is set such that the mean water level is nominally halfway up the cylinder. The entire device is loosely moored to the seabed.

In the presence of ocean waves, sea water will move up and down within the cylinder, producing the “oscillating water column”. This gives rise to air pressure within the cylinder alternating between positive and negative gauge pressure, which in turn causes air to alternately leave and enter the cylinder through the orifice. A bi-directional air turbine such as the

Siemens HydroAir Turbine converts the oscillating airflow into electric power for transport to shore or elsewhere by electric power cable.

The oscillating air pressure produces large up and down forces on the cylinder cap. These large forces are opposed through the rod to the large mass of water retained within the stabilizer which is located deep enough to be mostly free of wave influence and which provides the deep water reactance.

The cylinder and Stabilizer form a spring-mass system which has a vertical (heave) resonant frequency. The diameter of the cylinder largely determines the power rating of the device, while the size (and water mass within) of the stabilizer determines the resonant frequency which is chosen to be on the lower end of the wave frequency spectrum, to maximize the average power output of the device over a large span of time such as a year.

The upper portion of the device (the cylinder) moves laterally in surge with the waves. This motion is accommodated with minimal loading on the rod by having the stabilizer shaped as a sphere, allowing the entire device to rotate about the center of the stabilizer without rotating the seawater within the stabilizer, as if it were a ball joint.

A full scale device of this type shown below in Figure 2 may have the following dimensions - The cylinder may be 16 meters in diameter and 16 meters high, the stabilizer 24 meters in diameter, and have a draft of 94 meters. This technology is intended to significantly improve the economics of WECs, resulting from a large decrease in power/weight ratio, and increase in capacity factor, and an LCOE competitive with other forms for renewable energy such as wind and solar power. The total dry mass is estimated to be 94 tons.

Figure 2 shows the WEC in its intended operating position, with the bi-directional air turbine mounted on top. The mooring may be one, two, or three lines, with the attachment to the WEC most likely on the Stabilizer at the point of least motion. A power line will connect each WEC to a sea-bed mounted collection power cable.

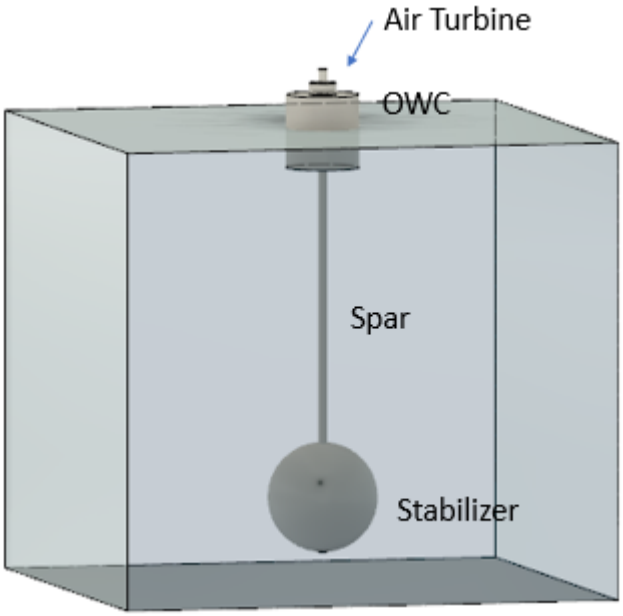

Figure 2: Depiction of full scale WEC

The Device Under Test (DUT), shown in Figure 3, consists of:

1. a quasi-spherical Stabilizer constructed from two thin-walled, 22 inch diameter plastic tubs, bolted together, at the bottom of the DUT,
2. a 9.91 foot long, 1.5 inch diameter, 0.0625 inch wall thickness stainless steel tubular shaft, functioning as the spar,
3. an 18 inch OD thin walled PVC tube, and 18 inch ID PVC cap, that define the OWC,
4. 8 inch diameter Styrofoam disks concentric to the top section of the spar which provide flotation,
5. a single 10 lb bar-bell weight at the bottom of the spar for ballast, in addition to the ballast supplied by the spar,
6. two pressure taps in the PVC cap to which to attach the OWC pressure sensors,
7. an orifice interface in the PVC cap, to be mated with either a 0.75 inch or a 1 inch diameter orifice plate, or with a cover plate to close the air chamber,
8. shaft collars to secure the various components of the spar.

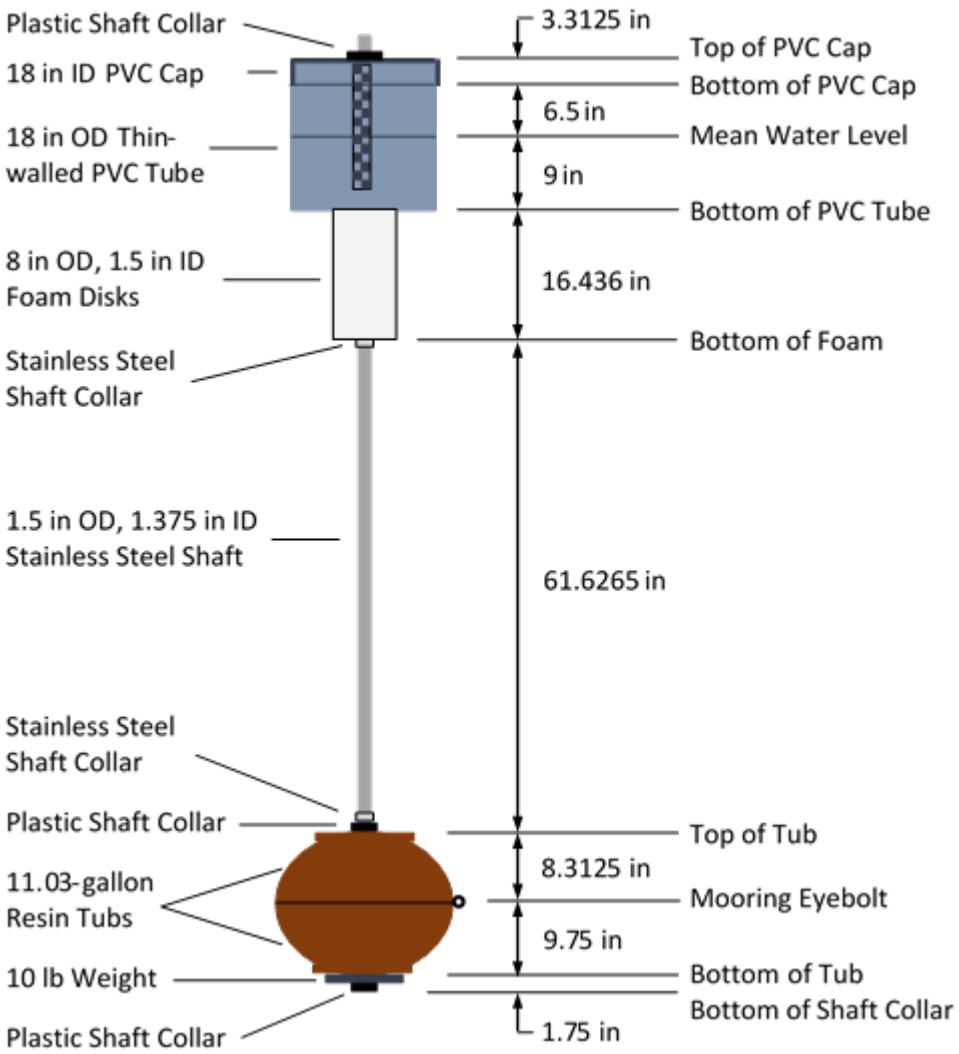

Figure 3: Dimensions of model

6 Work Plan

6.1 Experimental Setup, Data Acquisition System, and Instrumentation

6.1.1 Experimental Setup

The planned experimental setup is shown schematically in Figure 4 and Figure 5 below. The zero-offset location for the WEC will be over the center of the pit, 13.7 m from the wavemaker. The pit covers will be installed at the top of the pit and a mooring tower will be installed on the pit covers at the zero-offset location of the WEC. A single lightweight steel chain will be attached between the mooring tower and the WEC stabilizer. As the waves impinge on the WEC, a horizontal drift force will be set up that will force the WEC away from the mooring tower and tension the mooring cable.

The WEC will be instrumented to measure 6-degree-of-freedom motions using optical tracking, tension in the mooring cable, water level fluctuations at two locations in the interior water column, and air pressure in the chamber. The associated umbilical of instrument cables will be routed to an overhead plank with a horizontal slider so that the position of the umbilical can be remotely adjusted to a position that minimizes its parasitic force on the model. A soft extension spring attached vertically between the slider and a suitable point on the umbilical will further relieve the weight of the umbilical from being exerted on the WEC model.

The wavemaker drive signals for all wave conditions will be calibrated prior to installing the WEC model in the basin. The drive signals will be calibrated so as to achieve the specified wave conditions at the zero-offset location of the WEC model, as measured by a wave probe mounted at that location. During the wave calibration an additional two wave probes will be installed in the basin. One so-called "calibration" wave probe will be located approximately 1 m down wave of the zero-offset location representing a typical offset distance of the WEC under the wave drift force. The second wave probe will be a so-called "reference" wave probe mounted approximately 4 m to the side of the model zero-offset location. Upon completion of wave calibration, the two "calibration" wave probes will be removed while the "reference" wave probe will remain in place for the duration of the WEC tests.

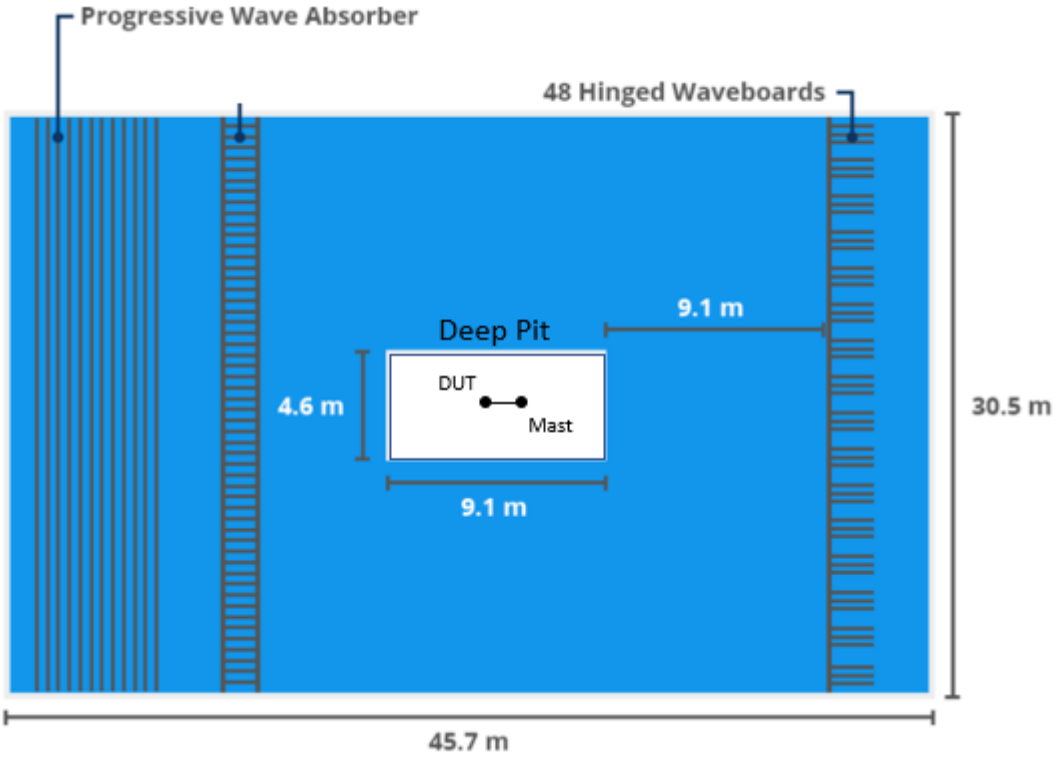

Figure 4: OTRC wave basin

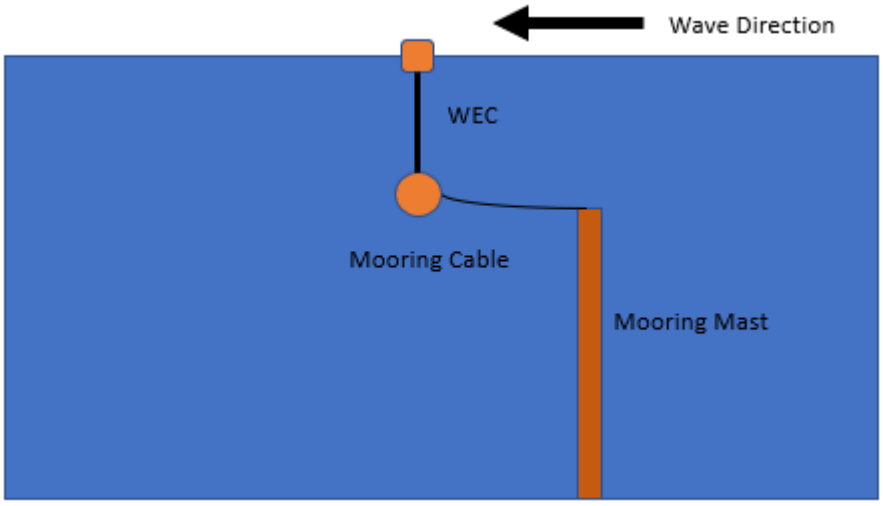

Figure 5: Mooring of the DUT

6.1.2 Data Acquisition System

The OTRC wave basin facility has an isolated GigE network for the data acquisition and control system used to run the wavemaker, acquire digital and analog sensor data, and stream digital video, all under common timing. A Dell VRTX Power Edge server with solid state hard drives provides the main computational horsepower as well as master timing control. Four other PC workstations in the control room are dedicated to various operator subsystems. A fifth PC in the engineer's office is for configuration of drive signals and data analysis. The data acquisition system includes two National Instruments controllers: one controller is capable of acquiring data from 16 digital channels and 112 analog channels at 2 kHz sampling rate, while the other controller is capable of acquiring data from 24 analog channels at 25 kHz sampling rate. All data is digitized with 16-bit resolution. The GEDAP software system is used for wavemaker control, data acquisition and data analysis.

6.1.3 Data Processing

The data processing that OTRC will undertake will be for quality control purposes. Following will be the scope of the data processing.

- For each incremental applied force, the surge static offset tests will be processed to compute standard statistics for each channel. The mean values of the surge, heave and pitch optical tracking channels and the mooring tension will be plotted against the applied offset force.
- For each heave and pitch decay test, the time series of decaying heave or pitch motion will be plotted and the equation for linearly damped free oscillation will be fit to the decay trace to identify the natural period and the damping level.
- For each regular wave test, the time series signals for all channels will be plotted and examined. A window of data containing at least 10 wave cycles will be identified and used for calculating standard statistics and RAOs for all relevant channels.
- For each irregular wave test, the time series signals for all channels will be plotted and the standard statistics for all channels will be tabulated. In addition, power spectra and extreme value distributions for all relevant channels will be plotted.

6.1.4 Instrumentation

Table 1 summarizes the instrumentation that will be deployed.

Table 1: Instrumentation

Channel	Measurement	Instrument	Wave Calibration	Model Tests	Range	Accuracy
1	Wavemaker Stroke	MLDT	√	√	± 0.1331 m	0.001 m
2	Cal Wave 1	Capacitance Wave Probe	√		1.2 m	0.8%
3	Cal Wave 2	Capacitance Wave Probe	√		1.2 m	0.8%
4	Ref Wave	Capacitance Wave Probe	√	√	1.2 m	0.8%
5	Surge	Qualisys Optical Tracking System		√	± 2 m	0.05%
6	Sway	Qualisys Optical Tracking System		√	± 2 m	0.05%
7	Heave	Qualisys Optical Tracking System		√	± 1 m	0.05%
8	Roll	Qualisys Optical Tracking System		√	± 15°	0.05%
9	Pitch	Qualisys Optical Tracking System		√	± 15°	0.05%
10	Yaw	Qualisys Optical Tracking System		√	± 15°	0.05%
11	Level 1	Capacitance Wave Probe		√	± 16 cm	0.8%
12	Level 2	Capacitance Wave Probe		√	± 16 cm	0.8%
13	Chamber Pressure 1	Differential Pressure Transducer		√	1 psi	0.08%
14	Chamber Pressure 2	Differential Pressure Transducer		√	1 psi	0.08%
15	Mooring Tension	U/W Tension/Compression Load Cell		√	25 lb	0.15%
16	Offset Force	U/W Tension/Compression Load Cell		√	25 lb	0.15%

All sensors will generate analog signals that will be sampled at 100 Hz with 16-bit resolution and low-pass filtered at 40 Hz corner frequency using 2-pole Butterworth filters. Apart from the Qualisys motion tracking system, all instruments will be calibrated prior to deployment by imposing a known series of displacements, loads or pressures and recording the voltage output. The Qualisys system self-calibrates using permanently-mounted reference optical markers whose locations relative to each other have been professionally surveyed.

6.2 Numerical Model Description

1. Develop boundary-element-method (BEM) model of scale-model OWC with deep-water reactance, provided a device geometry by Hiseas Energy. This model will be developed in an open-source BEM code, likely Capytaine, to facilitate future use. The BEM model will use a quadrangular mesh of sufficient resolution that will be developed from the provided geometry, and a basic mesh sensitivity study will be performed to ensure reasonable convergence of hydrodynamic parameters.

   Due to difficulties with internal free-surfaces in Capytaine, WAMIT

was used at partner request instead.

2. Build 1-DOF and simple 3/6-DOF model of OWC with idealized orifice in WEC-Sim to replicate laboratory experiments. This WEC-Sim model is informed by the BEM model coefficients, but includes additional physics omitted by the simpler BEM model.

3. Tune simulation based on laboratory results. Outputs of merit:

   - Power output vs. sea state
   - Dynamics vs. sea state
   - Structure loads
   - Internal water column dynamics

   The internal water column was measured, but no structural loads were measured aside from the mooring load. Tuning parameters:

   - Mooring parameters and complexity
   - Drag coefficients
   - Static/added masses
   - hydrostatic stiffnesses

4. If necessary: increase complexity of 3/6DOF model to include additional internal free-surface dynamics (assuming internal water height measurements are available). An idealized, but frequently realistic, model of a floating oscillating water column treats the internal free-surface of the water column as horizontal, orthogonal to the vertical direction of motion. If tank test data indicates that there is significant sloshing of the internal surface affecting device dynamics, these additional modes can be incorporated in the WEC-Sim model.

5. Enhance appropriate WEC-Sim model with realistic PTO model(s) and controllers. Fundamentally a Simulink block-set, WEC-Sim is well-suited to rapidly iterate controls approaches and PTO designs. Outputs of merit:

   - Power capture by sea-state
   - Control + PTO efficiency

6. Perform model design iterations/optimizations as directed and available.

6.3 Test and Analysis Matrix and Schedule

Table 2 outlines the planned test matrix. The model tests will be conducted at a scale of 1:35 and Froude scaling will be applied. The wave conditions are specified in full scale units.

The planned schedule for the tasks to be conducted by OTRC is provided in Figure 6 below.

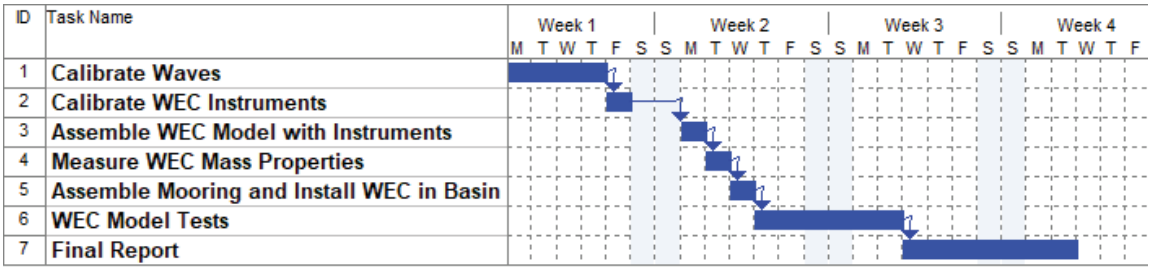

Figure 6: OTRC Project Schedule

Following is the planned schedule for tasks to be conducted by SNL.

- **Month 1**: From HiSeas provided geometry, develop a suitable mesh for BEM evaluation. Carry out the BEM analysis and mesh sensitivity study, analyze initial results.
- **Month 2**: Develop initial WEC-Sim model of device using the BEM hydrodynamic parameters. Begin analysis of tank-test data provided by OTRC to assess model agreement
- **Month 3**: Tune WEC-Sim model to align as well as possible with the OTRC data. Identify and quantify potential sources of disagreement. Provided adequate data is available, evaluate the need to expand WEC-Sim model to address additional internal sloshing mode.
- **Month 4**: If necessary, expand WEC-Sim model to incorporate additional water-column modes. Begin investigation of realistic PTOs and control approaches, quantifying power capture.
- **Month 5**: Continue investigation of PTOs and control approaches, focusing on high-performing candidates.
- **Month 6**: Iterate promising candidates as time allows. Provide estimates of performance metrics in various sea-states.

Table 2: OTRC Test Matrix

Test No.	Test Type	Orifice Diameter	Wave		
			H or Hs (m)	T or Tp (s)	DSig
Install WEC with Large Orifice					
CSGS	Surge Static Offsets	Large	-	-	-
CHVD	Heave Decay	Large	-	-	-
CRG1L	Regular Wave 1 Low	Large	1.5	8	RG1LA
CRG1H	Regular Wave 1 High	Large	3.0	8	RG1HA
CRG2L	Regular Wave 2 Low	Large	1.5	10	RG2L
CRG2H	Regular Wave 2 High	Large	3.0	10	RG2HA
CRG3L	Regular Wave 3 Low	Large	1.5	12	RG3LA
CRG3H	Regular Wave 3 High	Large	3.0	12	RG3HA
CRG4L	Regular Wave 4 Low	Large	1.5	14	RG4LA
CRG4H	Regular Wave 4 High	Large	3.0	14	RG4HA
CRG5L	Regular Wave 5 Low	Large	1.5	16	RG5LA
CRG5H	Regular Wave 5 High	Large	3.0	16	RG5HA
CWNL	White Noise Low	Large	1.5	5 - 25	WNLA
CWNH	White Noise High	Large	3.0	5 - 25	WNHB
CRW1	Irregular Wave 1	Large	1.5	8	RW1A
CRW2	Irregular Wave 2	Large	3.0	8	RW2A
CRW3	Irregular Wave 3	Large	1.5	12	RW3A
CRW4	Irregular Wave 4	Large	3.0	12	RW4A
Change to Small Orifice Diameter					
BHVD	Heave Decay	Small	-	-	-
BRG1L	Regular Wave 1 Low	Small	1.5	8	RG1LA
BRG1H	Regular Wave 1 High	Small	3.0	8	RG1HA
BRG2L	Regular Wave 2 Low	Small	1.5	10	RG2L
BRG2H	Regular Wave 2 High	Small	3.0	10	RG2HA
BRG3L	Regular Wave 3 Low	Small	1.5	12	RG3LA
BRG3H	Regular Wave 3 High	Small	3.0	12	RG3HA
BRG4L	Regular Wave 4 Low	Small	1.5	14	RG4LA
BRG4L	Regular Wave 4 High	Small	3.0	14	RG4HA
BRG5L	Regular Wave 5 Low	Small	1.5	16	RG5LA
BRG5H	Regular Wave 5 High	Small	3.0	16	RG5HA
BWNL	White Noise Low	Small	1.5	5 - 25	WNLA
BWNH	White Noise High	Small	3.0	5 - 25	WNHB
BRW1	Irregular Wave 1	Small	1.5	8	RW1A
BRW2	Irregular Wave 2	Small	3.0	8	RW2A
BRW3	Irregular Wave 3	Small	1.5	12	RW3A
BRW4	Irregular Wave 4	Small	3.0	12	RW4A
Change to Closed Orifice					
AHVD	Heave Decay	Closed	-	-	-
AWNL	White Noise Low	Closed	1.5	5 - 25	WNLA
AWNH	White Noise High	Closed	3.0	5 - 25	WNHB
Disconnect Mooring					
APTD	Pitch Decay	Closed	-	-	-
Reconnect Mooring and Change to Large Orifice Diameter					
CRWS	Survival Random Wave	Large	13.0	16	RWSA

6.4 Safety

All OTRC equipment will be operated by OTRC personnel. All heavy lifting, model installation and SCUBA diving operations will be conducted by OTRC personnel. Non-OTRC personnel will be restricted to designated observation areas within the basin. Under no circumstances are non-OTRC personnel permitted behind the wavemaker, on the work platform above the wave absorber, on the bridge spanning the basin, or in the workshops.

HiSeas Energy personnel may perform light assembly tasks on their WEC model in the staging area while OTRC technicians are present to ensure the work is being conducted safely. Upon request, OTRC technicians may provide mechanical and instrumentation support to HiSeas Energy as the WEC model is being prepared for installation in the basin.

6.5 Contingency Plans

The WEC model will be provided by HiSeas Energy, consequently OTRC cannot be responsible for any structural failure or loss of buoyancy of the model. HiSeas Energy will be financially responsible for any delays associated with unanticipated repairs to the WEC model.

Should there be any failure of OTRC equipment needed for testing, OTRC will, to the extent possible, promptly repair or replace the equipment before continuing as planned. Certain types of failures to major equipment (wavemaker, data acquisition system) may require extended periods of time to repair, in which case the WEC model will be temporarily removed from the basin until the equipment is repaired and the project can be re-started.

If SNL determines thay the data generated from tank testing is of limited utility/quality, it may not useful to tune the simulation to tank testing data, but simulation work can proceed presuming reasonable values for various tuning parameters and using the hydrodynamic data as estimated from BEM. In this way simulation work is not wholly dependent on the successful outcome of tank tests, and may be of some independent use.

6.6 Data Management, Processing, and Analysis

6.6.1 Data Management

Raw and processed test data will be stored on the Dell VRTX Power Edge server in the control room, which is backed up in real time to the university's cloud server. As part of the data processing, ASCII files will be created containing the time series data and tabulated basic statistics. In addition, data processing reports in the form of pdf files will be generated for each test and added to the archive. A separate archive containing photographs and digital video recordings from all wave tests will be assembled. A duplicate data archive will be assembled on Google drive and shared with HiSeas Energy and SNL for access to the data and processed results as they become available during the test program. At the conclusion of testing, the digital archive will constitute the primary deliverable.

6.6.2 Data Processing

As described in section 6.1.3, the data processing that OTRC will undertake will be for quality control purposes only. The data collected from each test will be processed shortly after the test is completed and the results will be examined to ensure they are consistent with expectations. Froude scaling for a scale ratio of 1:35 will be applied and all measurements will be reported in full scale units.

Following will be the scope of the data processing.

- For each incremental applied force, the surge static offset tests will be processed to compute standard statistics for each channel. The mean values of the surge, heave and pitch optical tracking channels and the mooring tension will be plotted against the applied offset force.
- For each heave and pitch decay test, the time series of decaying heave or pitch motion will be plotted and the equation for linearly damped free oscillation will be fit to the decay trace to identify the natural period and the damping level.
- For each regular wave test, the time series signals for all channels will be plotted and examined. A window of data containing at least 10 wave cycles will be identified and used for calculating standard statistics and RAOs for all relevant channels.

- For each irregular wave test, the time series signals for all channels will be plotted and the standard statistics for all channels will be tabulated. In addition, power spectra and extreme value distributions for all relevant channels will be plotted.

6.6.3 Data Analysis

Apart from examination of basic statistics, time series plots, power spectra and extreme value distributions for quality control purposes, data analysis will be limited to computation of RAOs from regular wave and white noise tests and to identification of natural periods and linear damping levels from decay traces. The analysis will be performed using GEDAP, which is an industry-standard software system licensed from the National Research Council of Canada for wavemaker control, data acquisition and data analysis. Froude scaling for a scale ratio of 1:35 will be applied and all measurements will be reported in full scale units.

7 Project Outcomes

7.1 Laboratory Results

7.1.1 WEC Mass and Hydrostatic Properties

Table 3 provides the measured mass and hydrostatic properties of the model WEC, reported in full scale units. The vertical elevation of the center of gravity, KG, is referenced to the keel and the gyradii Kxx, Kyy and Kzz are referenced to the center of gravity of the model. Kzz is the yaw radius of gyration.

The vertical buoyancy profile of the model WEC was measured by weighing it as it was lowered vertically, in stages, into the water. The resolution of the crane scale was 0.1 lb, model scale and the depth of submergence measurements were made to a precision of 1/16 inches, model scale. From the measured buoyancy profile, the total displacement and center of buoyancy of the hull were computed.

Table 3: WEC Model Mass and Hydrostatic Properties

Item	Units	Value
Weight	kN	10,451
KG	m	63.37
Kxx	m	42.94
Kyy	m	42.94
Kzz	m	5.40
Draft	m	95.01
Displacement	kN	10,551
Waterplane Area	m^2	49.35
KB	m	72.31
BM	m	0.45
GM	m	9.39

7.1.2 WEC Mooring

As indicated in section 6.1.1, the WEC was moored with a single line attached to a mooring tower. The mooring line consisted of a load cell segment followed by a length of anchor chain. The load cell segment was attached to the stabilizer on the WEC at the location indicated in Figure 3. The attachment of the anchor chain to the mooring tower was configured so that, in calm water, the WEC would float with its vertical z-axis located at the designated zero-offset location in the test area, and with its horizontal x-axis aligned with the direction of wave propagation. Table 4 provides the measured properties of the model mooring, reported in full scale units.

7.1.3 Instrumentation

Sign Conventions, Axes and Coordinate Systems

Two coordinate systems were employed: a basin-fixed coordinate system and a platform-fixed system. The right-handed, platform-fixed (X, Y, Z) coordinate system had its origin at mean water level on the vertical axis of the WEC, with positive Z up and positive X in the direction of wave propagation. The right-handed basin-fixed (north, west, Z) coordinate system was oriented with positive north upwave toward the wavemaker, positive west to the left when looking upwave, positive Z up.

The reference wave elevations were measured in the basin-fixed coordinate system. The platform motions were tracked by measuring the displacement of the origin of the platform-fixed coordinate system and the

Table 4: Model Mooring Properties

Item	Units	Value
Anchor Point		
Depth Below MWL	m	120
X-coordinate	m	-11.946
Y-coordinate	m	0
Hull Attachment Point		
Depth Below Waterline	m	84.788
X-coordinate	m	-11.946
Y-coordinate	m	0
Anchor Chain		
Length	m	35
Dry Weight per Unit Length	kN/m	2.29
Submerged Weight per Unit Length	kN/m	1.83
Load Cell Segment		
Length	m	6
Dry Weight per Unit Length	kN/m	9.73
Submerged Weight per Unit Length	kN/m	6.69

rotations of the platform-fixed coordinate axes relative to the calm water equilibrium location and vertical orientation of the WEC. Pressure and oscillating water column level were measured in the platform-fixed coordinate system.

Rotations about the platform-fixed axes followed the right-hand rule. Counter-clockwise rotation in the horizontal plane, when viewed from above, was positive yaw. Positive roll was when the platform positive y-axis went up. Positive pitch was when the platform positive x-axis went down.

Instrument Calibration

The instruments deployed during the test program are listed in Table 1. All instruments, besides the motion tracking system, were calibrated prior to use by imposing a known load or pressure or a measured displacement and recording the voltage output. All instrument calibration plots are provided in pdf format in the digital archive that accompanies this report.

Wavemaker Stroke

The wavemaker stroke is a measurement of the position of the pistons that drive the 48 hinged flaps. It is measured with a magneto-restrictive linear displacement transducer (MLDT). A stroke of zero corresponds to the wavemaker flaps standing straight up. Since all waves in this test

program were unidirectional, i.e. all flaps were moving in unison, it is typically necessary to monitor the motion of only one flap, normally flap 24 which is in line with the centerline of the pit. The stroke of the wavemaker was measured during each test to ensure that the waves run during testing were the same as those calibrated prior to installing the model in the basin. The unit for the stroke measurement is model scale meters.

Wave Elevation and Internal Water Level

The wave probes used to measure wave elevation and internal water level were of the capacitance type. These probes consist of a loop of thin insulated wire held taut by a supporting rod. The wire insulation serves as a capacitor between the conducting copper wire and the water. The capacitance varies linearly with changes in water elevation.

A total of three wave probes were used to measure water level variations in the wave basin during wave calibration. The positions of these probes relative to the center of the pit (i.e. the center of the test area) are shown in Figure 7 in model scale units. During the test program, the two "Cal" wave probes on the North-South centerline were removed to make way for the model. The reference wave probe on the basin west side of the pit remained in the basin throughout the test program.

Two capacitance wave probes were mounted on the WEC model to measure the level oscillations of the internal water column. The locations of these probes are shown in Figure 8 and listed in Table 5.

The wave elevation probes were set to read zero value when the water was calm. The internal water level probes were set to read zero when the WEC was trim and at the draft line. Positive values represented water surface elevations higher on the probe. The units for the wave elevation and internal water level measurements are full scale meters.

Table 5: Internal Water Level Probe and Air Pressure Tap Locations

Instrument	Platform X (m)	Platform Y (m)
Air Pres 1	-2.275	5.845
Air Pres 2	2.415	-5.670
Level 1	-7.315	0
Level 2	7.000	0

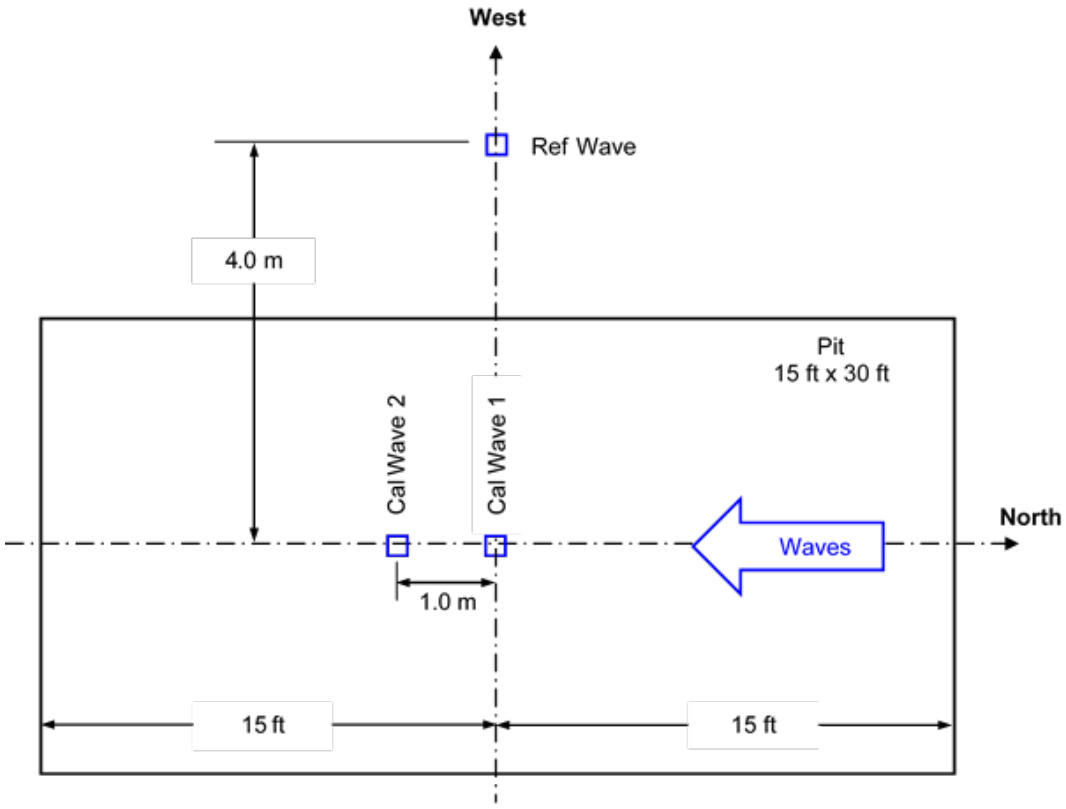

Figure 7: Wave Probe Locations for Wave Calibration

Platform Motions

The model motions were measured using a Qualisys optical tracking system. The system uses an array of six cameras mounted on the east side of the basin tracking a set of 4 infrared light-emitting targets mounted on the WEC model. The array of Qualisys tracking targets mounted on the model is evident in Figure 8. The Qualisys system measures rigid body motions in all 6 degrees of freedom (DOF). The system was configured to calculate and output the motions of the platform-fixed coordinate system, defined above. The zero conditions for surge, sway, heave, roll, pitch and yaw were taken with the platform moored at the specified draft, with a level trim and list, in calm water.

Positive surge is in the platform-fixed positive X-direction. Positive sway is in the platform-fixed positive Y-direction. Positive heave is up. Positive roll is rotation in which the platform-fixed Y axis goes up. Positive pitch is rotation in which the platform-fixed X axis goes down. Positive yaw is counterclockwise when viewed from above.

The units for surge, sway and heave are full scale meters. The units for

roll, pitch and yaw are degrees.

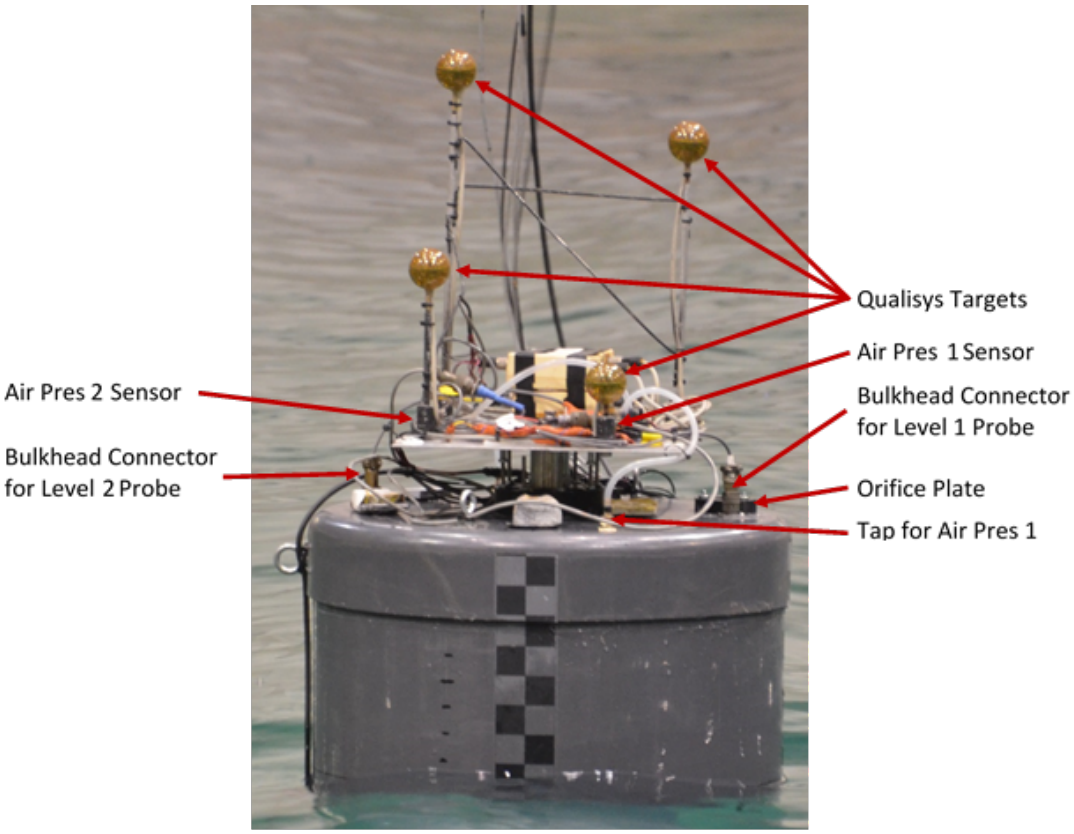

Figure 8: Top of WEC Instrumentation

Chamber Air Pressure

The air pressure in the air chamber was measured using differential pressure transducers. Two All Sensors ADCA series amplified low pressure sensors were mounted on the mounting plate for the Qualisys optical tracking targets and connected to the air chamber cap through small diameter white flexible tubes (Figure 8). One of the air pressure sensors (labeled "Air Pres 1") was rated to 25.0 mbar and the other (labeled "Air Pres 2") was rated to 12.5 mbar. Table 5 provides the locations of the taps for the air pressure sensors.

Zero values of pressure correspond to atmospheric pressure. Positive values represent increased pressure. The units for the force measurements are full scale kilo-Pascals (kPa).

Mooring Tension and Static Offset Force

An inline, submersible, tension/compression load cell was used to measure

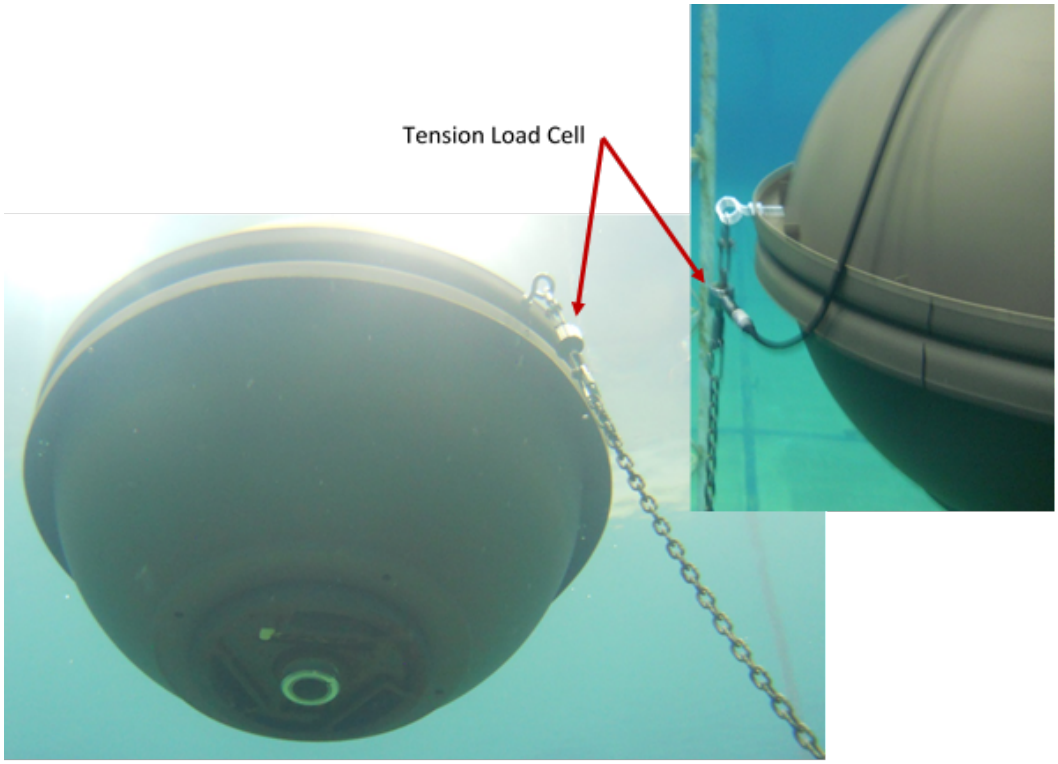

Figure 9: Mooring Tension Load Cell

the tension in the mooring line at the attachment to the WEC stabilizer. The mooring load cell segment is shown in Figure 9. A similar load cell was used to measure the tension in the string used to exert horizontal forces on the model for the static offset tests. Zero values were set when the instruments were unloaded. Positive values represent increased tension. The units for the force measurements are full scale kilo-Newtons (kN).

7.1.4 Wave Calibration

Wavemaker

Wave generation was provided by a bank of 48 hinged flaps that were controlled to produce uni-directional waves. To protect the wavemaker from potential overloading, it used a high frequency cut-off at 2 Hz (model scale). At 1:35 scale this corresponds to 0.338 Hz (2.96 sec period) prototype. Wave absorption was accomplished at the opposite end of the basin by a progressive absorber consisting of a series of metal screens of decreasing mesh size.

Wave Probe Layout

A total of two calibration probes and one reference probe were used during

the wave calibration tests. Calibration of all waves was completed before the model was installed in the basin. The calibration probes were removed for the tests with the WEC. The Ref Wave reference probe remained in place throughout the project. The locations of the wave probes are shown in Figure 7. The zero offset reference location for the WEC model was at the Cal Wave 1 probe location.

Target Wave Conditions

Ten regular wave drive signals and seven irregular wave drive signals were calibrated. The irregular wave conditions comprised four operational seastates, one survival seastate, and two white noise wave trains. The irregular wave drive signals were calibrated using the Random Phase Method, whereby only the phases of the Fourier components are randomized. In this technique the amplitudes of the Fourier components are selected so that the spectral density of the smooth target wave elevation spectrum is matched.

Each regular wave train was run for 1065 sec, full scale, which for the longest (16 sec period) waves represents over 60 wave cycles. For each of 5 regular wave periods, regular wave trains were calibrated for a full scale height of 1.5 m and 3.0 m. The 5 regular wave periods were 8, 10.12, 14 and 16 seconds, full scale.

All irregular wave trains were calibrated for 3-hours duration, full scale (not including a 2-minute, model scale ramp-up period at the beginning of the drive signal). The parameters of the Bretschneider spectra for the operational and survival seastates were:

- Hs = 1.5 m, Tp = 8 sec,
- Hs = 3.0 m, Tp = 8 sec,
- Hs = 1.5 m, Tp = 12 sec,
- Hs = 3.0 m, Tp = 12 sec,
- Hs = 13.0 m, Tp = 16 sec.

The white noise wave trains were calibrated for periods ranging from 5 to 25 seconds. The target significant wave heights were 1.5 m and 3.0 m. Due to wave breaking, the white noise wave spectra could not be of constant amplitude all the way to the high frequency cutoff. Therefore,

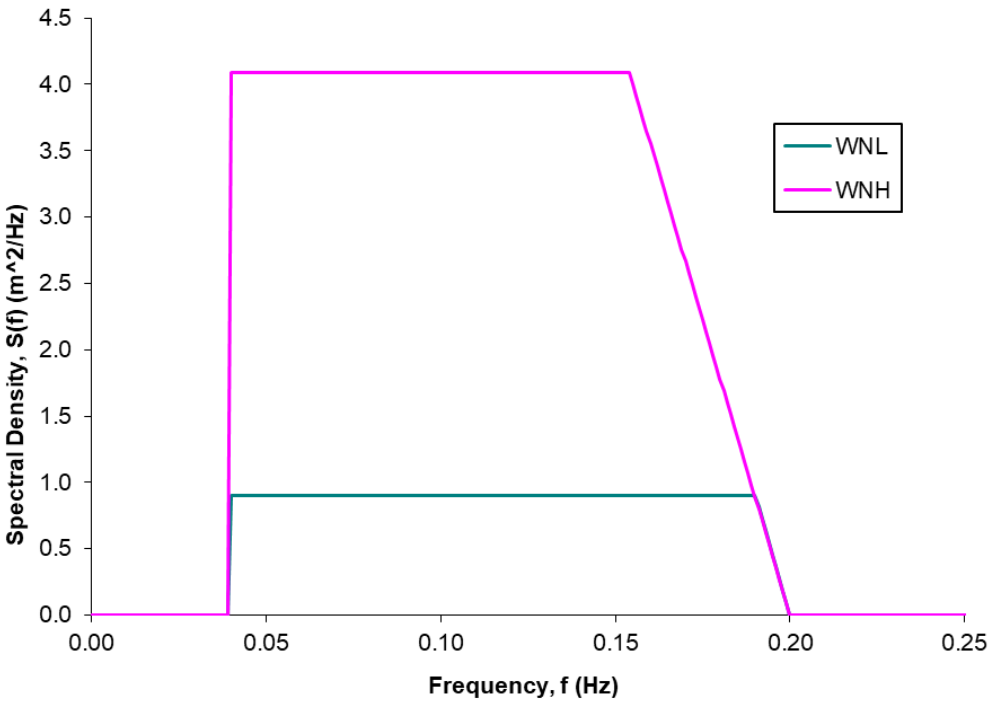

Figure 10: Target White Noise Spectra

the target white noise spectra were linearly tapered to zero at the high frequency end, as shown in Figure 10. The frequency at which the linear taper started was 0.190 Hz for the Hs = 1.5 m spectrum and 0.154 Hz for the Hs = 3 m spectrum.

Regular Wave Calibration Results

For purposes of comparing with the target values, the measured regular wave height and period were determined by analyzing a data window selected to avoid the leading wave transient effects and the first arrival of partially reflected waves from the wave absorber. Table 6 identifies the data window and summarizes the associated wave measurements for all of the calibrated regular wave conditions.

For each regular wave calibration test, summary tables of standard statistics as well as time series plots, for both the entire test and the data window, are provided in the digital archive that accompanies this report.

Irregular Wave Calibration Results

Table 7 summarizes the wave measurements for all of the calibrated irregular wave conditions.

For each irregular wave calibration test, summary tables of standard

Table 6: Regular Wave Calibration Summary

Test	DSig	Target		Window		Stroke Std Dev (m)	Ref Wave	
		H (m)	T (s)	Start (s)	End (s)		WAV_HAVD (m)	WAV_TAVD (s)
RG1LA_001	RG1LA	1.5	8	190	320	0.001819	1.481	7.992
RG1HA_001	RG1HA	3.0	8	190	320	0.003648	3.127	8.003
RG2L_001	RG2L	1.5	10	170	290	0.002173	1.315	9.988
RG2HA_001	RG2HA	3.0	10	170	290	0.004213	2.823	10.00
RG3LA_001	RG3LA	1.5	12	150	262	0.002396	1.472	12.00
RG3HA_001	RG3HA	3.0	12	150	262	0.004788	3.021	12.01
RG4LA_001	RG4LA	1.5	14	135	237	0.002980	1.497	13.97
RG4HA_001	RG4HA	3.0	14	135	237	0.005954	3.009	13.99
RG5LA_001	RG5LA	1.5	16	120	212	0.003407	1.444	16.24
RG5HA_001	RG5HA	3.0	16	120	212	0.007215	3.027	16.03

Test	Target		Cal Wave 1				Cal Wave 2			
	H (m)	T (s)	WAV_ HAVD (m)	HAV Error (%)	WAV_ TAVD (s)	TAV Error (s)	WAV_ HAVD (m)	HAV Error (%)	WAV_ TAVD (s)	TAV Error (s)
RG1LA_001	1.5	8	1.538	2.5%	7.999	-0.001	1.533	2.2%	8.000	0.000
RG1HA_001	3.0	8	2.927	-2.4%	8.003	0.003	2.913	-2.9%	7.999	-0.001
RG2L_001	1.5	10	1.490	-0.7%	9.983	-0.017	1.436	-4.3%	10.02	0.020
RG2HA_001	3.0	10	2.966	-1.1%	9.998	-0.002	2.944	-1.9%	10.00	0.000
RG3LA_001	1.5	12	1.507	0.5%	11.98	-0.02	1.478	-1.5%	11.97	-0.03
RG3HA_001	3.0	12	2.956	-1.5%	12.01	0.01	2.956	-1.5%	11.98	-0.02
RG4LA_001	1.5	14	1.511	0.7%	13.97	-0.03	1.553	3.5%	13.97	-0.03
RG4HA_001	3.0	14	3.016	0.5%	14.00	0.00	2.992	-0.3%	13.99	-0.01
RG5LA_001	1.5	16	1.505	0.3%	16.03	0.03	1.507	0.5%	16.04	0.04
RG5HA_001	3.0	16	3.032	1.1%	16.04	0.04	3.094	3.1%	16.03	0.03

statistics as well as time series plots, plots of power spectra and Weibull plots of extreme value distributions are provided in the digital archive that accompanies this report. For each wave calibration test, a single pdf file containing all of the processed results is provided.

Note that in Table 7 `H_MAX` and `AC_MAX` are the 3-hour most probable maximum values of the wave height and crest elevation, as provided on the Weibull plots. The measured values of the spectral peak period, Tp, are based on smoothing the power spectrum to 0.005 Hz resolution.

7.1.5 Test Procedures

Wave Calibration

The wave calibration tests were each initiated when the basin was calm. "Calm" was defined to be when the peak-to-peak variation of the wave probes was less than 0.1 m, full scale, over an interval of 30 seconds, model scale. The wave probes were "zeroed" before each test when the "calm" criterion was met.

Data collection for the regular waves commenced as soon as the wavemaker began to move. The initial transient in both the waves was captured in the test record. The duration of the data acquisition interval was 17.75 minutes, full scale or 3 minutes, model scale.

Data collection for irregular waves commenced two minutes, model scale, after the wavemaker started. This was to provide sufficient time for the initial transients in both the waves and the platform responses to decay to insignificance. The duration of the data acquisition interval was three hours, full scale (30.43 minutes, model scale).

Surge Static Offset Tests

Surge static offsets tests were conducted with the large (1-inch diameter) orifice in place. The surge static offset tests were executed by applying an increasing horizontal force in the basin south (positive platform X) direction through a lightweight string attached at (X,Y,Z) = (8.0 m, 0, 6.9 m). For each static offset test the model was moved to a location and a brief interval was allotted for the motions to settle, then data was acquired for a minimum of a thirty-second interval, model scale.

Decay Tests

Free vibration (decay) tests were conducted in heave and pitch in order

Table 7: Irregular Wave Calibration Summary

Test	DSig	Target		Stroke Std Dev (m)	Ref Wave	
		Hs (m)	Tp (s)		WAV_HMO (m)	SPEC_TP (s)
WNLA_001	WNLA	1.5	5 - 25	0.002481	1.560	
WNHB_001	WNHB	3.0	5 - 25	0.004732	3.147	
RW1A_001	RW1A	1.5	8	0.001183	1.521	7.230
RW2A_001	RW2A	3.0	8	0.002467	3.105	6.856
RW3A_001	RW3A	1.5	12	0.001687	1.522	12.05
RW4A_001	RW4A	3.0	12	0.003314	3.101	12.05
RWSA_001	RWSA	13.0	16	0.015220	12.84	15.91

Test	Target		Cal Wave 1					
	Hs (m)	Tp (s)	WAV_ HMO (m)	HMO Error (%)	SPEC _TP (s)	Tp Error (s)	H_MAX (m)	AC_MAX (m)
WNLA_001	1.5	5 - 25	1.542	2.8%			2.711	1.533
WNHB_001	3.0	5 - 25	3.020	0.7%			5.251	3.330
RW1A_001	1.5	8	1.481	-1.3%	8.115	0.115	2.871	1.691
RW2A_001	3.0	8	3.028	0.9%	7.797	-0.203	5.523	3.779
RW3A_001	1.5	12	1.526	1.7%	12.05	0.05	3.051	1.684
RW4A_001	3.0	12	3.053	1.8%	12.05	0.05	5.745	3.515
RWSA_001	13.0	16	13.14	1.1%	15.91	-0.09	21.90	14.43

Test	Target		Cal Wave 2					
	Hs (m)	Tp (s)	WAV_ HMO (m)	HMO Error (%)	SPEC _TP (s)	Tp Error (s)	H_MAX (m)	AC_MAX (m)
WNLA_001	1.5	5 - 25	1.587	5.8%			2.697	1.632
WNHB_001	3.0	5 - 25	3.012	0.4%			5.290	3.210
RW1A_001	1.5	8	1.511	0.7%	9.248	1.248	2.753	1.636
RW2A_001	3.0	8	3.048	1.6%	8.461	0.461	5.541	3.663
RW3A_001	1.5	12	1.565	4.3%	11.70	-0.30	2.858	1.729
RW4A_001	3.0	12	3.048	1.6%	11.70	-0.30	5.220	3.084
RWSA_001	13.0	16	13.06	0.5%	15.91	-0.09	21.99	14.61

to determine the natural period and equivalent linear (viscous) damping for each mode of motion. Free vibration in heave was initiated by pushing down on the model at the plan center. Pitch was induced by pulling horizontally in opposing directions by strings attached to the mooring eyebolt on the stabilizer and the static offset test pull point at the top of the spar, briefly holding the inclined position, then releasing the strings. The heave decay tests were conducted with the WEC in the moored condition. For the pitch decay tests, the WEC was un-moored and freely floating.

Heave decay tests were conducted with both the small and large orifices and with the orifice opening closed. A single pitch decay tests was conducted, with the orifice opening closed.

Calm Tests

Short tests were conducted when it was determined that the wave basin was "calm" and the WEC model was at rest. "Calm" was when the peak-to-peak variation of the reference wave probe was less than 0.1 m, full scale, over an interval of 30 seconds, model scale. All data channels were recorded for a minimum of 30 seconds, model scale. The Calm test data may be used to determine the at-rest values of the measurements immediately prior to, or after, a wave test.

Regular Wave Tests

Regular wave tests with the WEC model were conducted for a duration of 3 minutes, model scale or 17.75 minutes, full scale. The drive signals created during the wave calibration tests were used. Data acquisition commenced immediately upon the start of the wavemaker. The initial transient of the waves and platform responses was captured in the time series. Five seconds, model scale, prior to commencement of data acquisition the video title was recorded. Upon commencement of data acquisition, the video title was switched to a view of the WEC model.

Irregular Wave Tests

Irregular wave tests (which includes white noise tests) with the WEC model were conducted for the full scale equivalent of three hours. The drive signals developed during the wave calibration tests were used. Data acquisition commenced two minutes, model scale after the waves started. This initial interval allowed the initial transients in the waves and the plat-

form responses to decay to insignificance. During the initial two-minute interval, the umbilical of electronic cables running from the overhead plank to the model was adjusted to minimize its effect on the platform responses. Five seconds, model scale, prior to commencement of data acquisition the video title was recorded. Upon commencement of data acquisition, the video title was switched to a view of the WEC model. For the purposes of time series analysis, the data from each irregular wave test is considered to be stationary over the full three-hour record.

7.1.6 Description of Data Products

A National Instruments (NI) data acquisition system with the GEDAP software package acquired data for all channels. The data channels were sampled at 100 Hz model scale (16.903 Hz prototype scale) and low pass filtered with 2-pole Butterworth filters with 30 Hz corner frequency.

Preliminary data reduction and analysis for all tests was conducted using the OTRC's integrated wave generation, data acquisition and data analysis software. Electronic data files containing the summary statistics tables (in ASCII format) and times series of all data channels are included in the digital archive that accompanies this report. The summary statistics files are named *Testname.s1*. The ASCII time series files are named *Testname.dt1*. Header information for the time series files is provided in the file *hdr.dt1* included in each ASCII Time Series folder.

In addition to the basic univariate statistics, a number of wave specific statistics were calculated for the wave calibration tests. These can be found in ASCII summary tables and in the pdf reports.

- `WAV_HMO` is an estimate of the significant wave height based on the spectral moment m_0 ($\texttt{WAV\_HMO} = 4\sqrt{m_0}$),
- `SPEC_TP` is the spectral peak period corresponding to the peak frequency of the spectrum,
- `WAV_HMAXD` is the maximum wave height in the wave record, with individual waves determined by zero downcrossing,
- `WAV_AC_MAX` is the maximum wave crest elevation in the wave record, with individual waves determined by zero downcrossing,
- `SPEC_M0` is the zeroth moment m_0 of the spectrum $S(f)$. m_0 has the units of u^2 where u is the units of the time series signal,

- `SPEC_M1` is the first moment m_1 of the spectrum $S(f)$. m_1 has the units of u^2/s^1 where u is the units of the time series signal and $s =$ seconds,
- `SPEC_M2` is the second moment m_2 of the spectrum $S(f)$. m_2 has the units of u^2/s^2 where u is the units of the time series signal and $s =$ seconds.
- `SPEC_M3` is the third moment m_3 of the spectrum $S(f)$. m_3 has the units of u^2/s^3 where u is the units of the time series signal and $s =$ seconds,
- `SPEC_M4` is the fourth moment m_4 of the spectrum $S(f)$. m_4 has the units of u^2/s^4 where u is the units of the time series signal and $s =$ seconds,
- `ZCA_NWD` is the number of zero downcrossing wave cycles detected in the wave record.

For the irregular wave calibration tests and the WEC seakeeping tests, additional analysis products include spectral plots and extreme value analysis.

Spectral Analysis

The GEDAP spectral analysis tools estimate the variance spectral density of a time series by smoothing the periodogram of the total record. The time series is first multiplied by a data window to reduce leakage prior to computing the periodogram. The final spectral density estimates are obtained by using a simple moving average filter to smooth the periodogram. The length of the filter is chosen to obtain a specified number of degrees of freedom per spectral estimate. The degrees of freedom for each spectral estimate are listed on the plots.

Extreme Value Analysis

Zero-crossing analysis was performed to find the "crests" (positive excursion from the mean) and "troughs" (negative excursion from the mean) of the fluctuating signals. In general only "crests" were examined for the wave elevation probes while both "crests" and "troughs" were examined for the WEC motions, oscillating water column elevations, air chamber pressures, and line tension.

The exceedance probability for each recorded "crest" or "trough" was computed from the order starting with the largest and descending to the smallest. The exceedance probability for a particular measured event is

$$|\text{Exceedance Probability}| = \frac{I - 1/2}{|\text{number of crests}|} \tag{1}$$

where I = *rank of the event.* $I = 1$ for the largest event and I = *number of waves* for the smallest event. The measured exceedance distribution is then plotted on a log-log scale. A model is then fit to the exceedance distribution with additional weight given to the tail of the distribution. This is typically done by fitting a line to a set number of the largest events (20 events in most cases). With the parameters for the tail, the 3-hour event is interpolated based on the average zero-crossing period.

Response Amplitude Operators

The tests with the WEC in waves were processed to derive response amplitude operators (RAOs) for all relevant channels using the associated wave calibration tests as the input to the (assumed) linear system. The RAO analysis was performed using standard tools in the GEDAP software suite.

For each regular wave test, the same time window that was used for a zero-crossing analysis of the corresponding wave calibration test to determine the measured wave height and period (see Table 6) was also used for the analysis of the RAO for each response. Monochromatic sine waves were fit to the input wave elevation window and to the output response window. The amplitude, frequency and phase angle of the sine wave fit to each window was identified. The amplitude of the RAO was obtained by dividing the amplitude of the sine wave fit to the response by the amplitude of the sine wave fit to the wave elevation. The RAO phase shift was obtained by subtracting the phase angle of the sine wave fit to the wave elevation from the phase angle of the sine wave fit to the response. For each regular wave test, the results of this RAO analysis are tabulated in the ASCII *Testname.S5* files archived in the digital database that accompanies this report.

For each irregular wave test, cross-spectral analysis of the input (wave elevation) and output (response) time series for the entire test record was performed to determine the RAO amplitude and phase, as well as the

linear coherence between the input and output signals as a function of frequency. For each white noise wave test, the results of this RAO analysis are tabulated in the ASCII *Testname.rao*, *Testname.pha* and *Testname.coh* files archived in the digital archive that accompanies this report. The column labels for these ASCII files are contained in the files *hdr.rao*, *hdr.pha* and *hdr.coh*, respectively. In addition, plots of the RAOs are provided in the pdf files *Testname.rao*. The RAO files are collected in separate folders included in the digital archive that accompanies this report.

7.1.7 Visual Documentation

Still Photography

Digital still photographs were taken during model assembly, outfitting, ballasting, installation and testing. A complete set of photographs is provided on the digital archive that accompanies this report.

Video

Video was shot of the wave tests. Video was not shot of the various wave calibration tests, static offset tests, decay tests or calm tests. Two video cameras were employed for this test program and the video feed from the two cameras was recorded in separate video files. The video from the cameras was recorded in 1080i format at 59.94 fields per sec (and interlaced at 29.97 frames per sec).

One camera was located on the east side of the basin looking horizontally at the model so that the portion above the waves was viewed in profile. In this view the waves traveled from right to left. The second camera was submerged and mounted on a tripod on the wave basin floor east of the pit, and provided an upward view of the keel and east side (positive Y side) of the model.

A short title precedes each test, identifying the test name and the primary environmental conditions. A time stamp, showing the model scale time and date, appears at the bottom of the screen. This time stamp is synchronized to the time of the data acquisition computer. The start time of each test is recorded and displayed in the summary statistics files, *.s1, in the digital archive that accompanies this report.

7.1.8 Surge Static Offset Test Results

Surge static offset tests were conducted by attaching a string to the model at platform (X,Y,Z) = (8.0 m, 0, 6.9 m) and pulling horizontally toward basin south (i.e. the positive force direction). The large orifice was installed for the static offset tests.

The measured static offset curves are provided in Figures 11 through 14. An OrcaFlex model of the WEC with the mooring system was exercised to generate reference results for comparison with the measured static offset curves. The agreement between the measurements and the OrcaFlex model results validates the WEC mass and buoyancy properties and the mooring properties reported in sections 7.1.1 and 7.1.2.

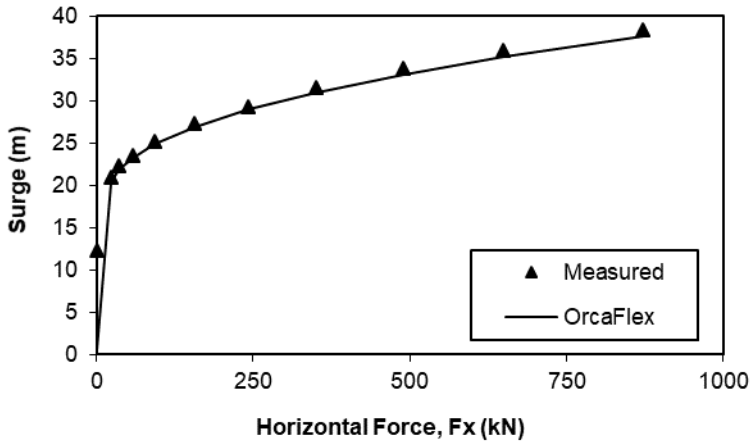

Figure 11: Surge Static Offset Test - Force vs Surge

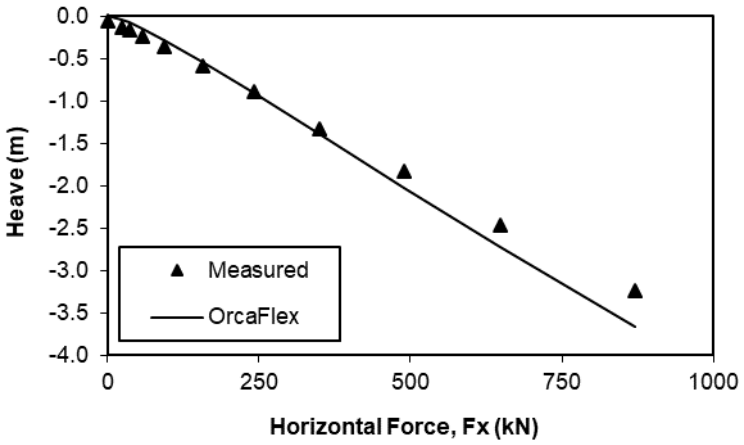

Figure 12: Surge Static Offset Test - Force vs Heave

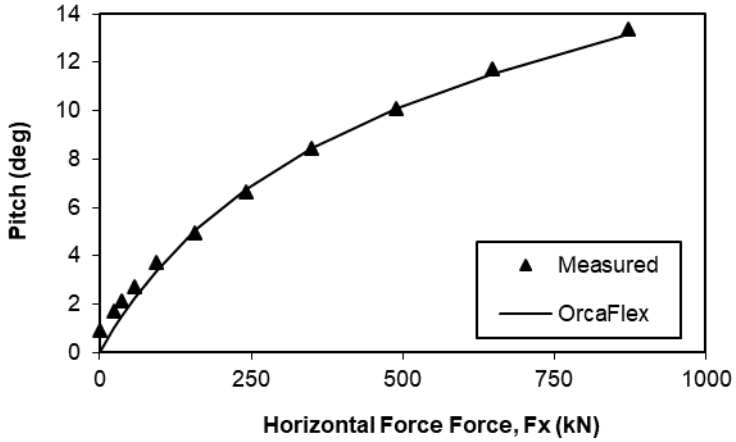

Figure 13: Surge Static Offset Test - Force vs Pitch

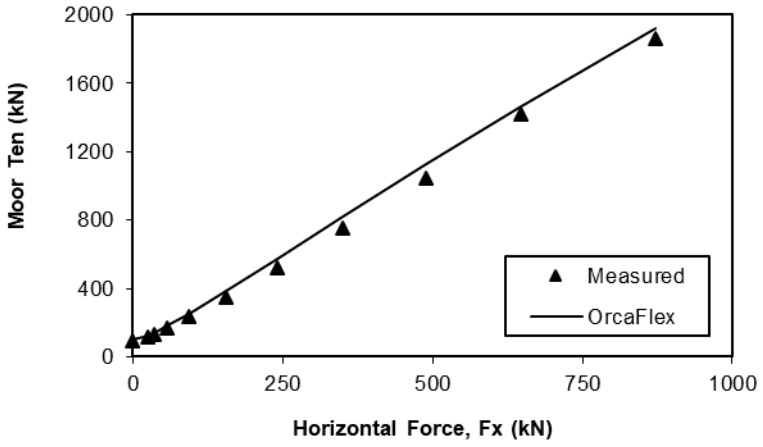

Figure 14: Surge Static Offset Test - Force vs Mooring Tension

7.1.9 Decay Test Results

In accordance with the test matrix, heave decay tests were conducted for the three orifice conditions (small. large and closed) with the WEC moored, and pitch decay tests were conducted for the closed orifice condition with the WEC free=floating. With the closed orifice it was possible to induce uncoupled, single degree-of-freedom motions, and to analyze the decay traces in order to identify the natural period and linear (viscous) damping level. The results are presented in Tables 8 and 9 below.

Table 8: Analysis of Heave Decay Test with Closed Orifice

Test	Mode	Start (s)	Stop (s)	Initial Amplitude (m)	Period (sec)	Linear Damping (%)	Average Period (sec)	Average Damping (%)
AVHD_001	Heave	53	163	3.0	14.17	4.06%		
		1131	1241	3.5	14.19	4.07%		
		2236	2346	3.5	14.20	4.26%		
		3377	3487	2.5	14.09	3.76%		
							14.16	**4.04%**

Table 9: Analysis of Pitch Decay Test with Closed Orifice

Test	Mode	Start (s)	Stop (s)	Initial Amplitude (deg)	Period (sec)	Linear Damping (%)	Average Period (sec)	Average Damping (%)
APTD_001	Pitch	510	810	7.0	63.63	9.24%		
		1450	1670	4.5	63.38	9.63%		
		3326	3625	5.5	63.35	9.96%		
							63.45	**9.61%**

For the heave decay tests with either the large or small orifice, the heave decay trace was indicative of a 2-degree-of-freedom response, evidently due to coupling with the stiffness and damping provided by the internal air flow through the orifice. For these tests a more advanced analysis using a numerical model such as WEC-Sim is needed to sort out the natural periods and damping levels associated with each response mode.

7.1.10 Response Amplitude Operators

The regular and white noise tests were processed to derive response amplitude operators (RAOs) for all relevant channels using the associated wave calibration tests as the input to the (assumed) linear system. The RAO analysis was performed using standard tools in the GEDAP software suite.

For each relevant response, and for each orifice size, a single plot comparing the regular wave RAOs with the RAOs derived from each of the two white noise wave conditions was generated. Figures 15 to 21 show the effect of the incident wave amplitude on the response RAOs. Where apparent, the vertical separation between the RAO curves for the low and high white noise energy levels, and between the RAO points for the low and high regular wave amplitude levels, are indicative of the extent to which the system is responding nonlinearly.

Figures 22 to 28 show the effect of the orifice size on the response RAOs derived from the white noise tests. The orifice size has little effect on the surge and pitch RAOs but a large effect on the internal water level RAOs and on the heave and air pressure RAOs near the heave natural period.

a) Large Orifice

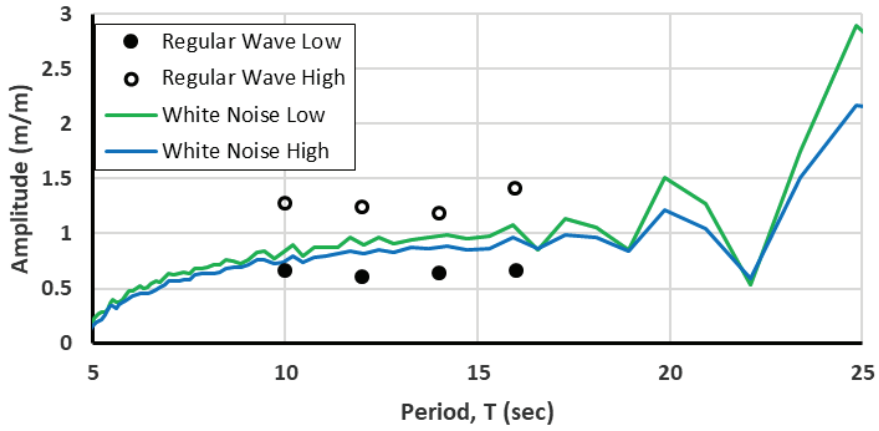

b) Small Orifice

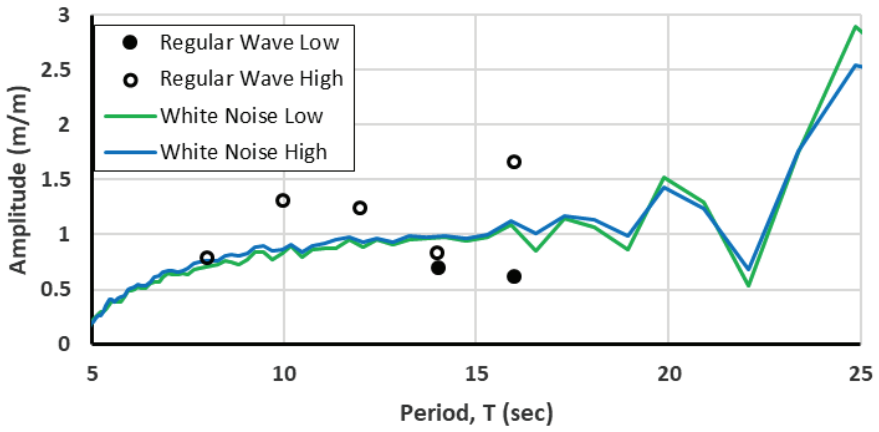

c) Closed Orifice

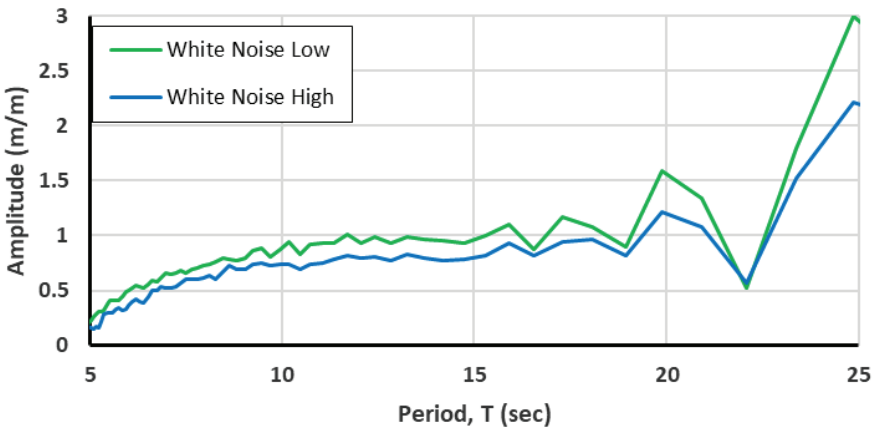

Figure 15: Surge RAOs

a) Large Orifice

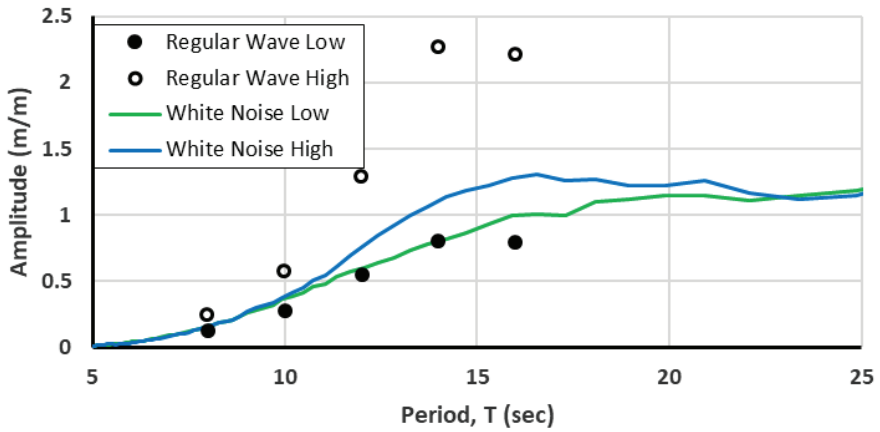

b) Small Orifice

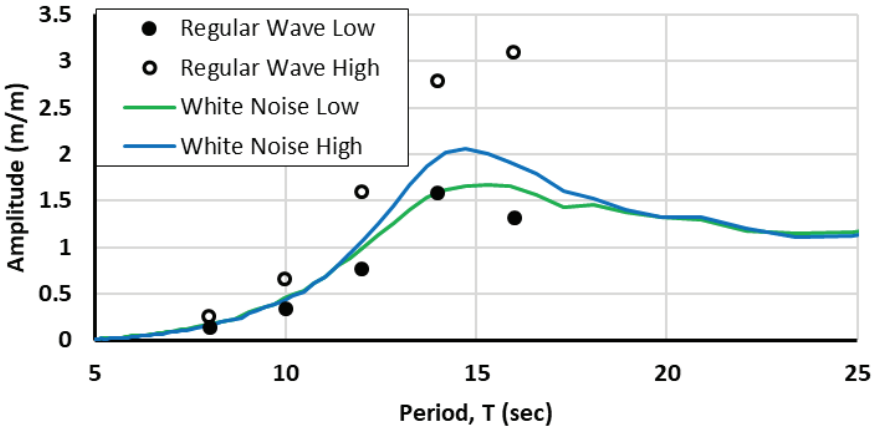

c) Closed Orifice

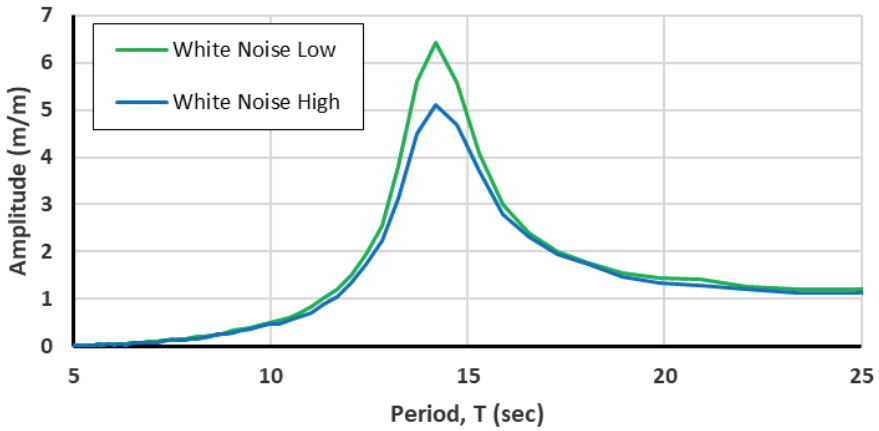

Figure 16: Heave RAOs

a) Large Orifice

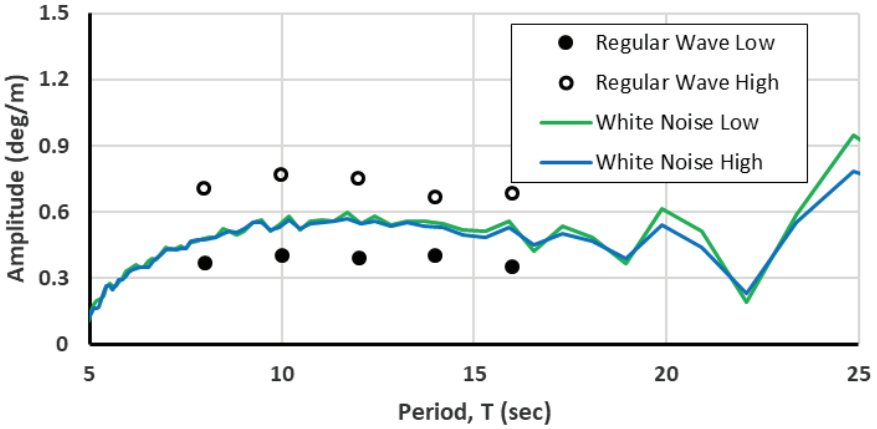

b) Small Orifice

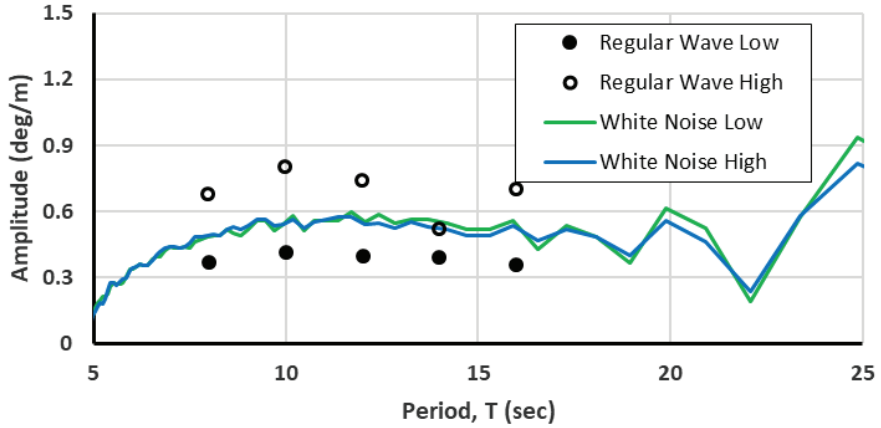

c) Closed Orifice

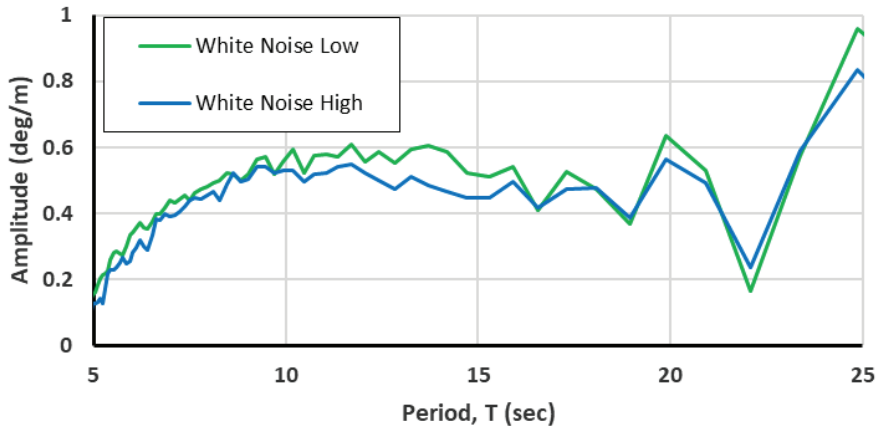

Figure 17: Pitch RAOs

a) Large Orifice

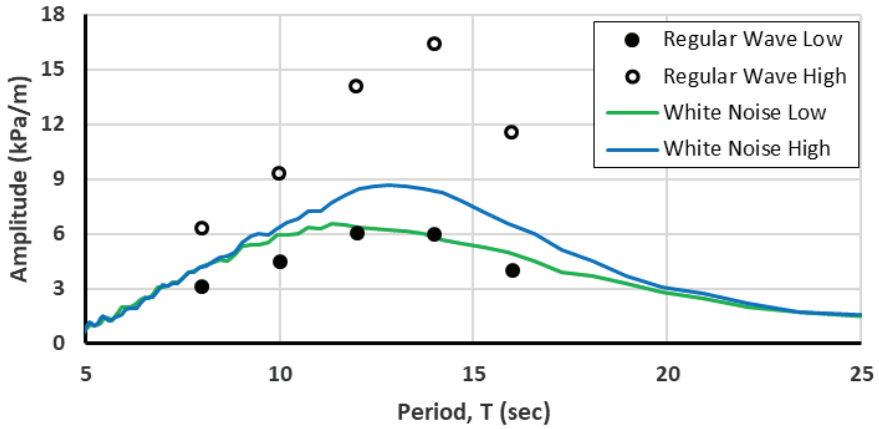

b) Small Orifice

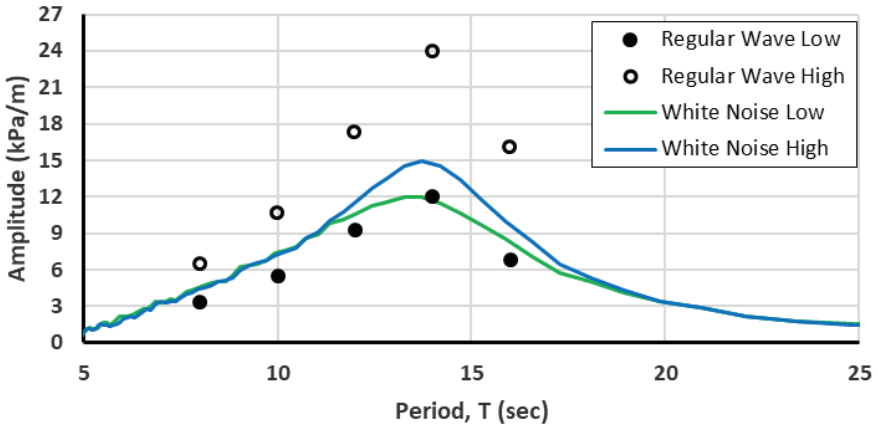

c) Closed Orifice

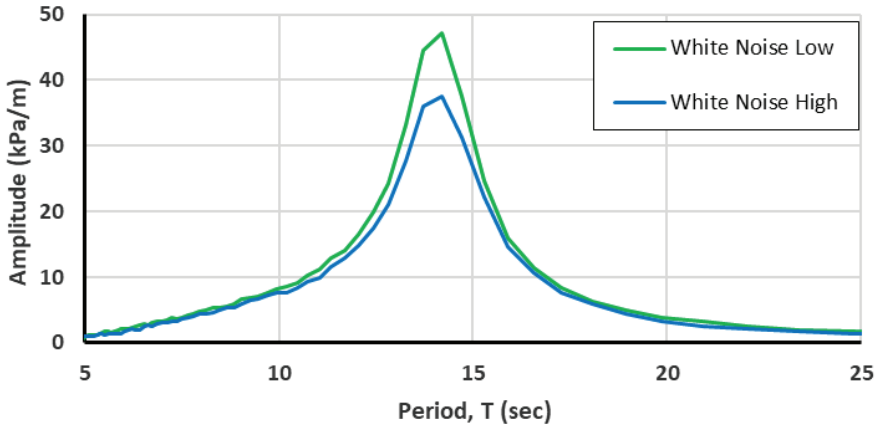

Figure 18: Air Pressure 1 RAOs

a) Large Orifice

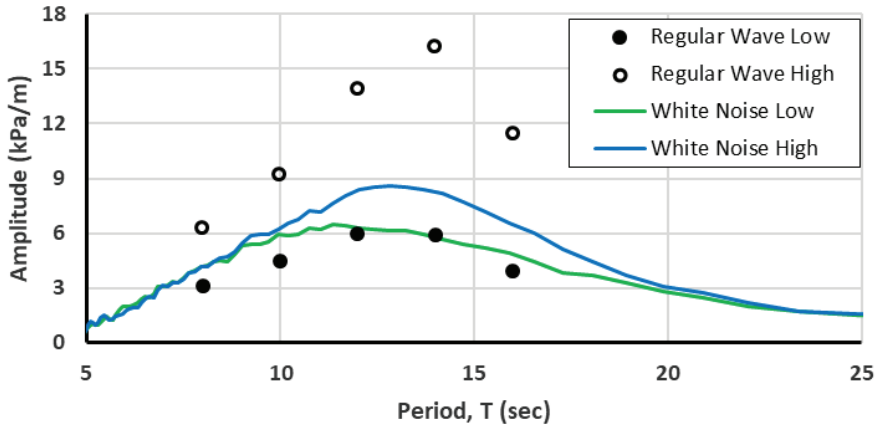

b) Small Orifice

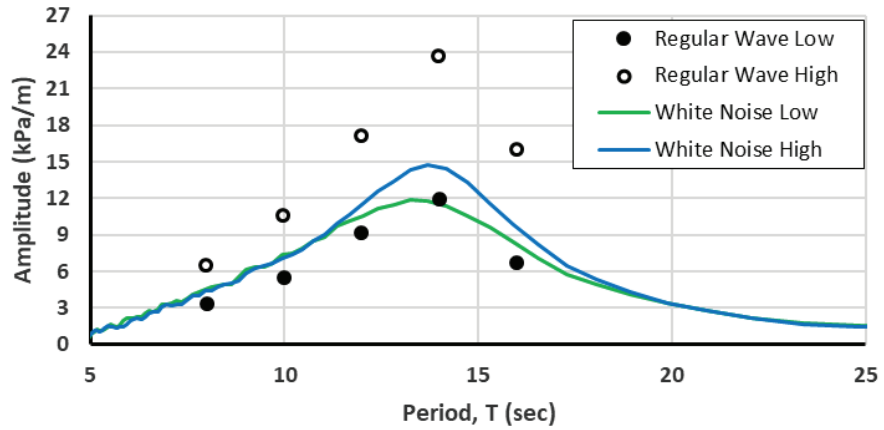

c) Closed Orifice

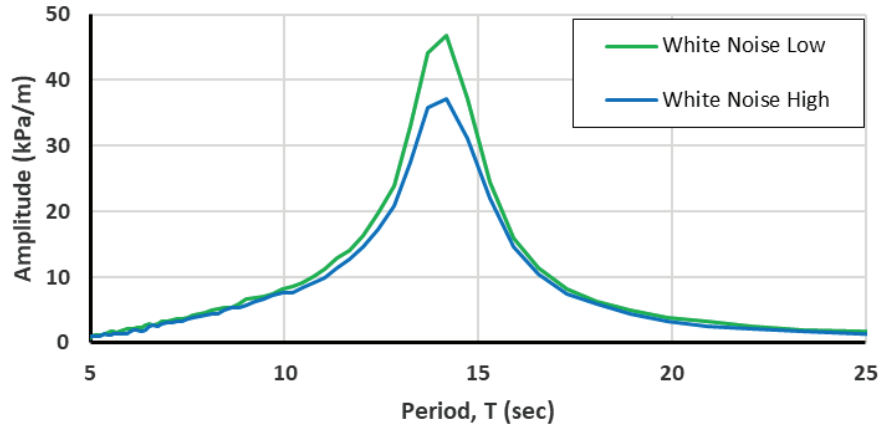

Figure 19: Air Pressure 2 RAOs

a) Large Orifice

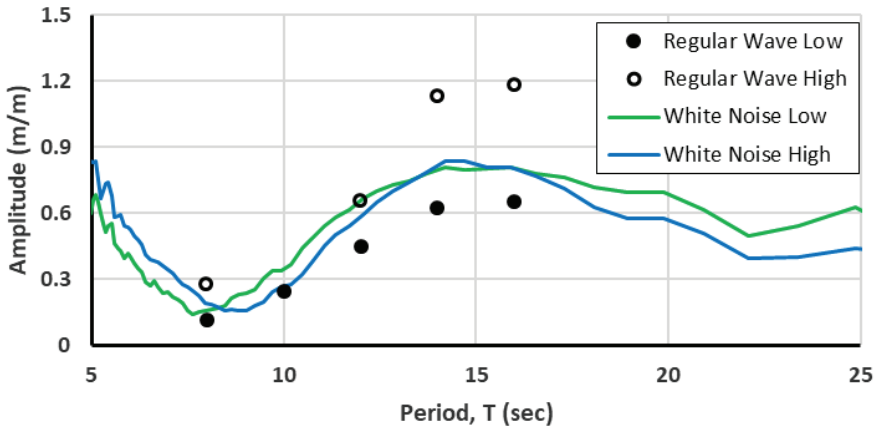

b) Small Orifice

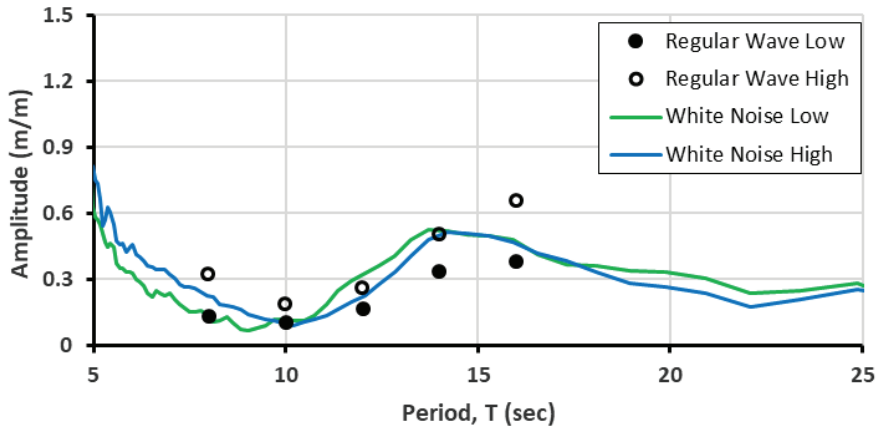

c) Closed Orifice

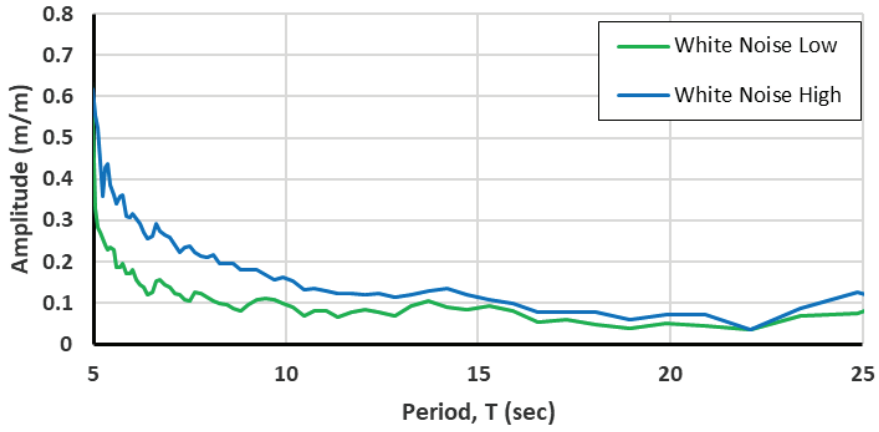

Figure 20: Water Level 1 RAOs

a) Large Orifice

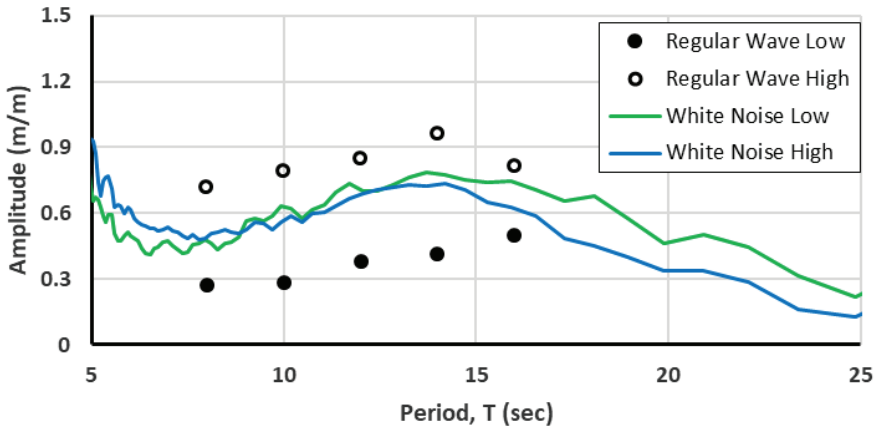

b) Small Orifice

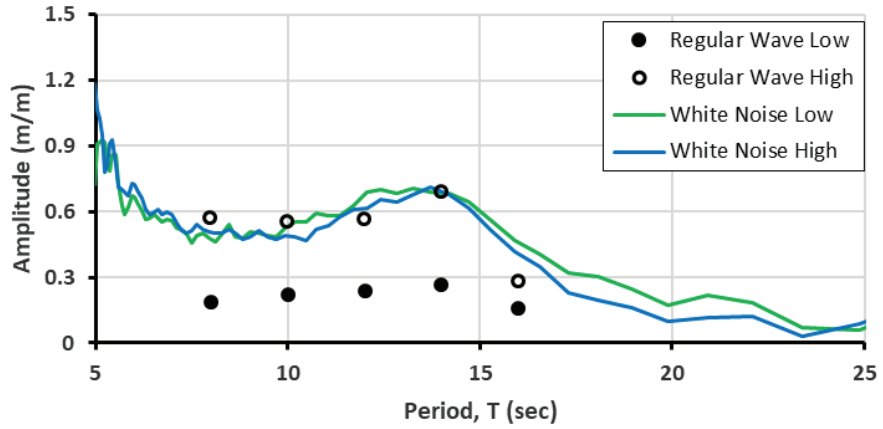

c) Closed Orifice

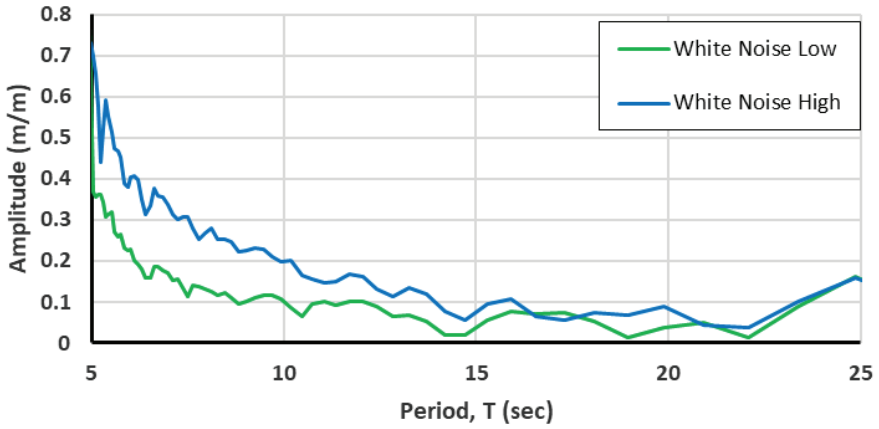

Figure 21: Water Level 2 RAOs

a) Low White Noise

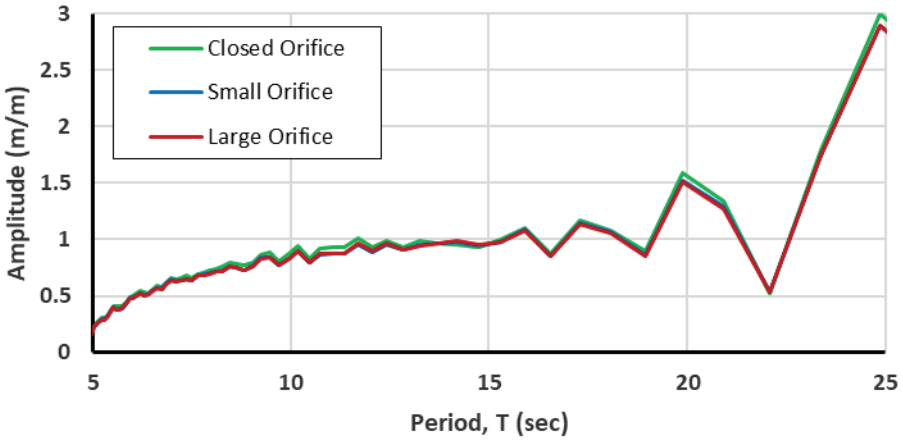

b) High White Noise

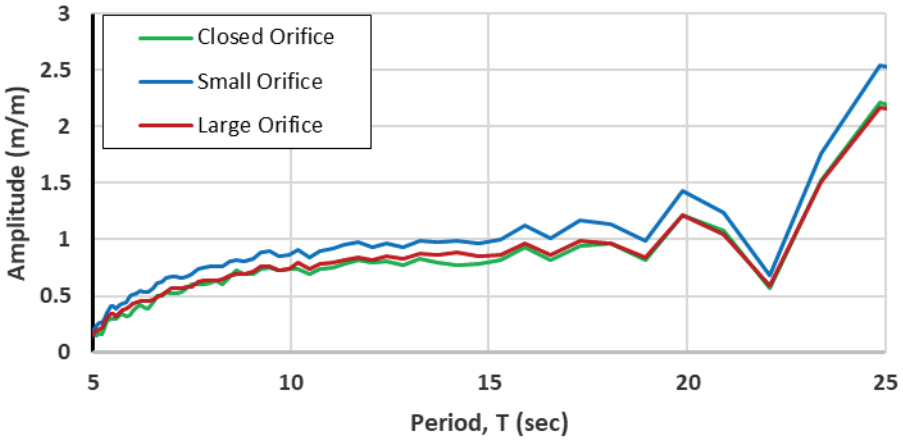

Figure 22: Effect of Orifice Size on Surge RAOs

a) Low White Noise

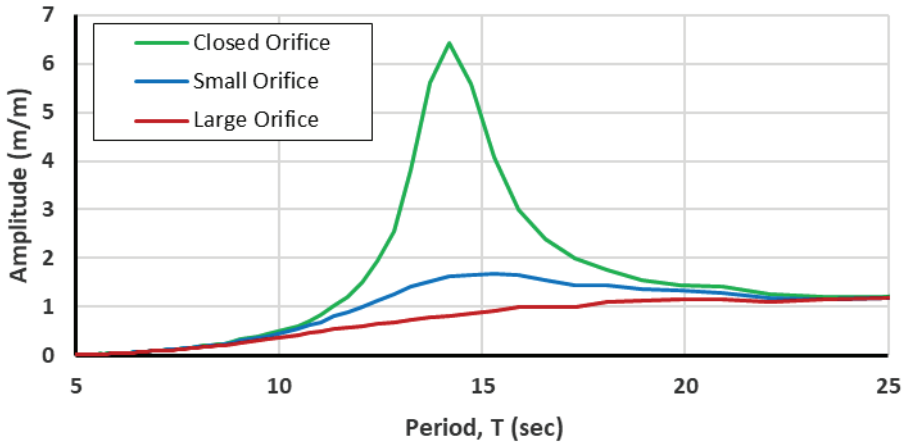

b) High White Noise

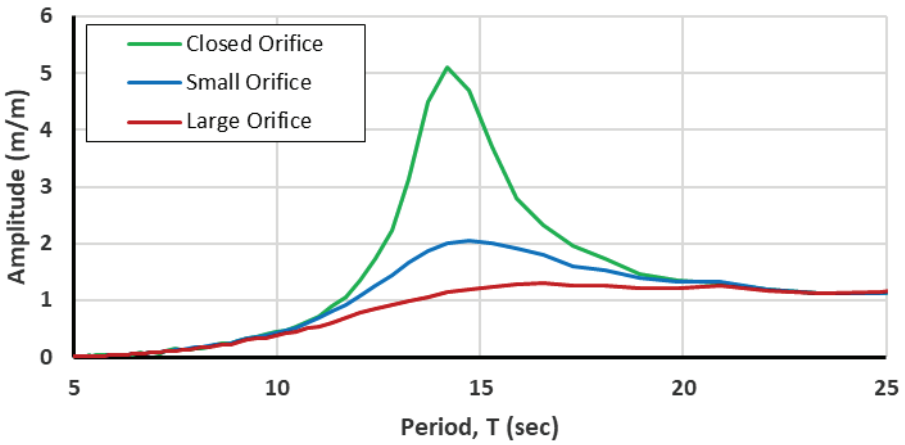

Figure 23: Effect of Orifice Size on Heave RAOs

a) Low White Noise

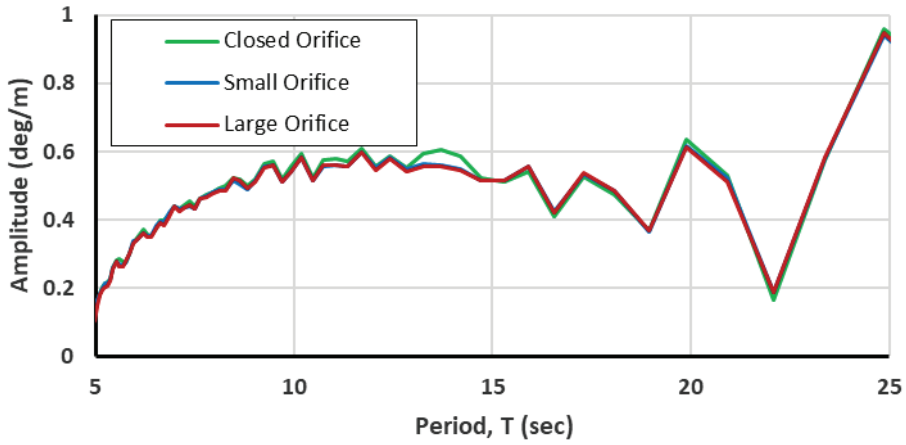

b) High White Noise

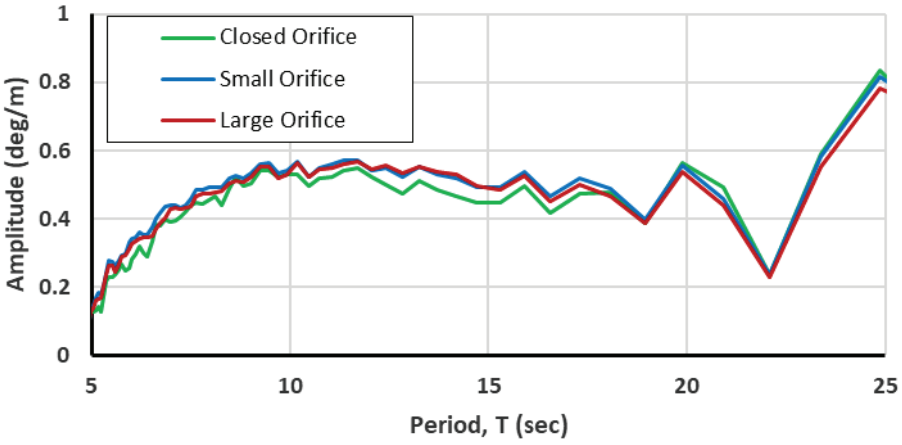

Figure 24: Effect of Orifice Size on Pitch RAOs

a) Low White Noise

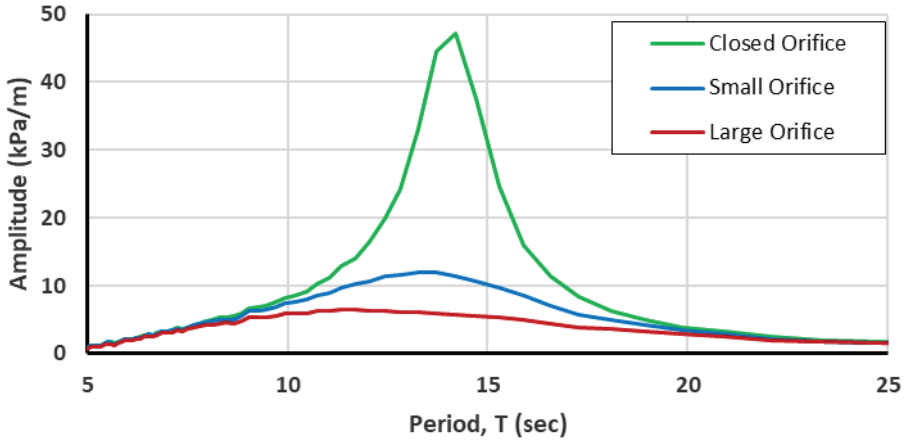

b) High White Noise

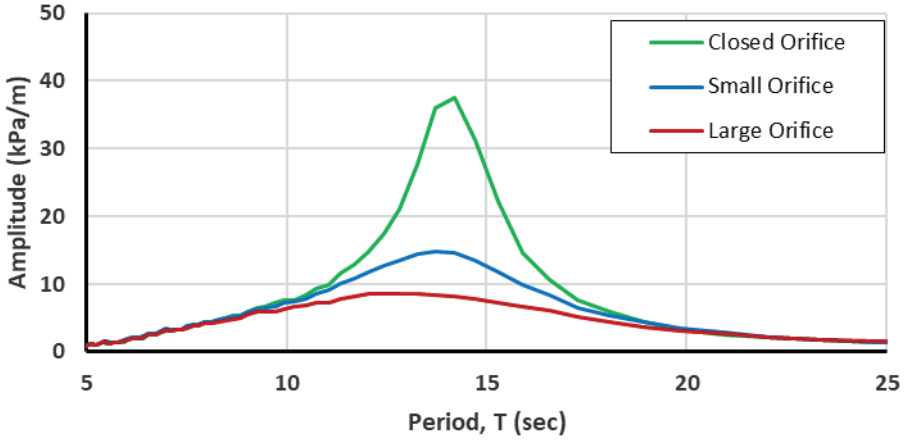

Figure 25: Effect of Orifice Size on Air Pressure 1 RAOs

a) Low White Noise

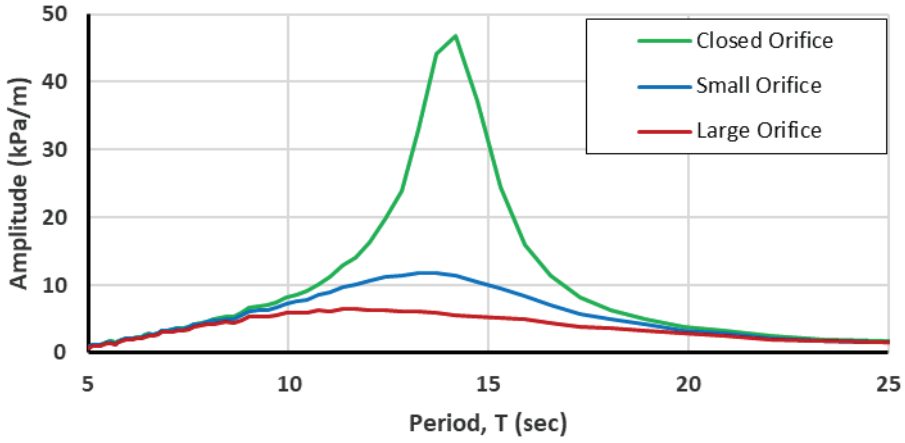

b) High White Noise

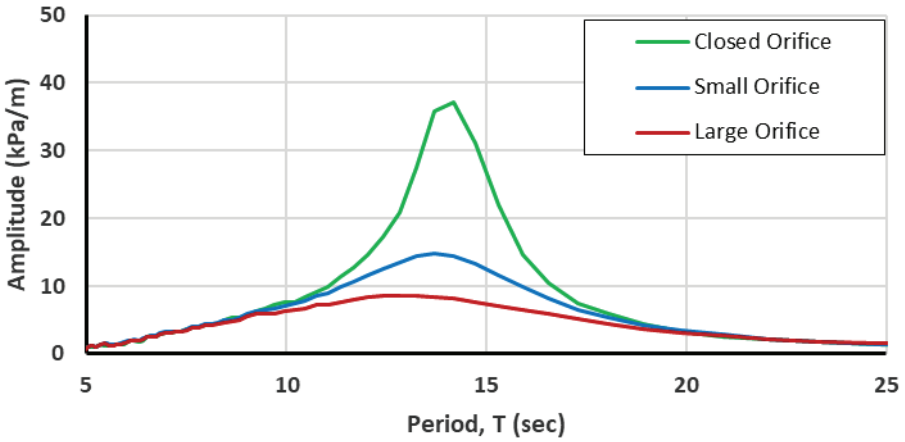

Figure 26: Effect of Orifice Size on Air Pressure 2 RAOs

a) Low White Noise

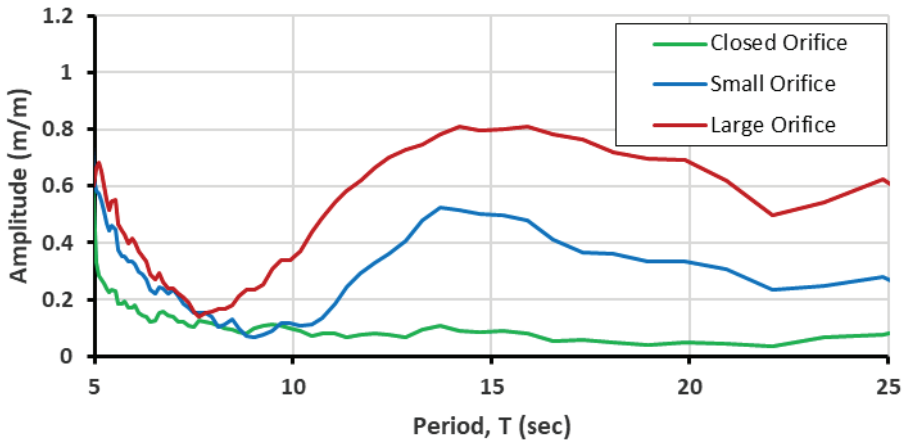

b) High White Noise

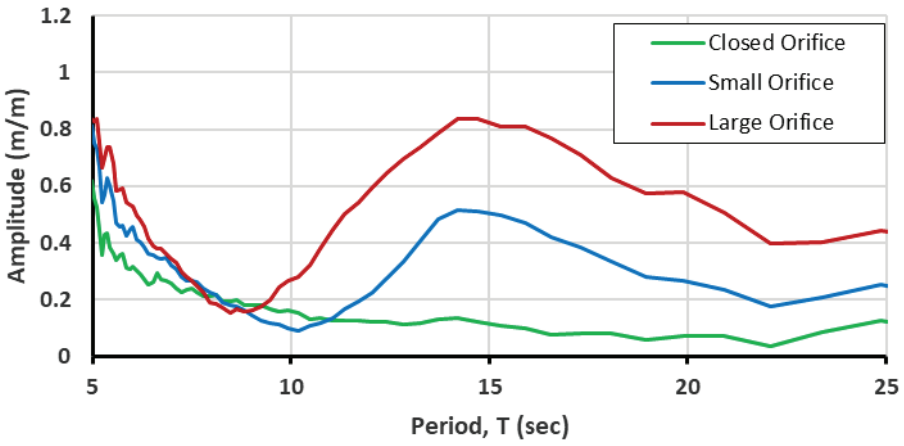

Figure 27: Effect of Orifice Size on Water Level 1 RAOs

a) Low White Noise

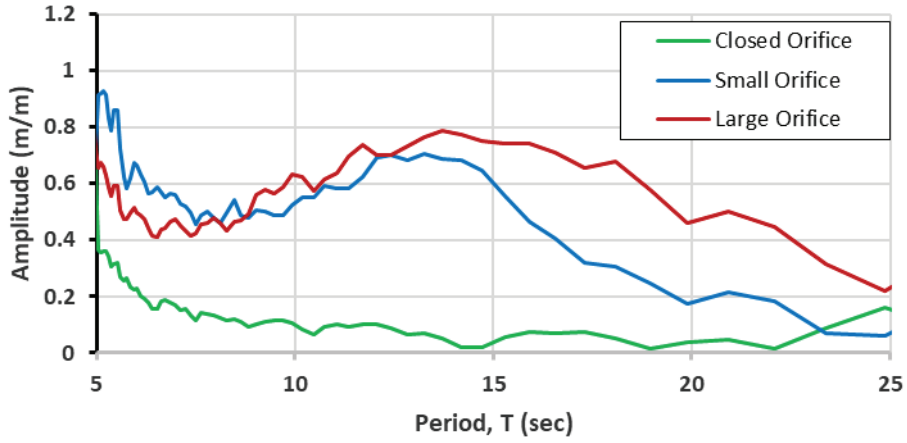

b) High White Noise

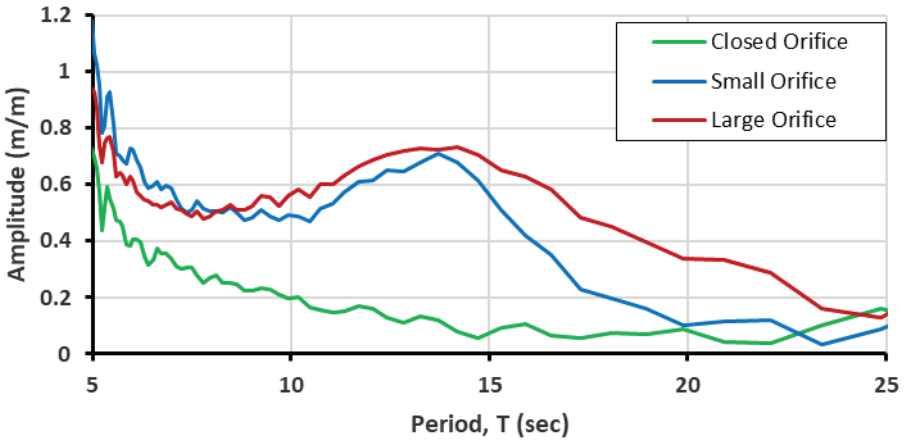

Figure 28: Effect of Orifice Size on Water Level 2 RAOs

7.1.11 Data Transfer

The digital archive that accompanies this report may be accessed at `https://drive.google.com/drive/folders/1GqtutO3w9qI0PQvEpgojaTEF3fHe6stS?usp=sharing`. The contents of the digital archive include:

- Wave Calibration: Test Summary Statistics and Time Series in ASCII format and Processed Test Results (power spectra, Weibull plots, time series plots, RAOs) in pdf format
  - Regular Waves
  - White Noise
  - Irregular Waves
- Large Orifice Tests: Test Summary Statistics, RAOs and Time Series in ASCII format, Processed Test Results (power spectra, Weibull plots, time series plots, RAOs) in pdf format, and video recordings in .mov format
  - Surge Static Offset Test
  - Heave Decay Test
  - Regular Waves
  - White Noise
  - Irregular Waves
- Small Orifice Tests: Test Summary Statistics, RAOs and Time Series in ASCII format, Processed Test Results (power spectra, Weibull plots, time series plots, RAOs) in pdf format, and video recordings in .mov format
  - Heave Decay Test
  - Regular Waves
  - White Noise
  - Irregular Waves
- Closed Orifice Tests: Test Summary Statistics, RAOs and Time Series in ASCII format, Processed Test Results (power spectra, Weibull plots, time series plots, RAOs) in pdf format, and video recordings in .mov format

  - Heave Decay Test
  - Pitch Decay Test
  - White Noise
- Photographs
  - Wave Calibration
  - Model Outfitting
  - Dip Test
  - Bifilar Pendulum
  - Model Installation
  - Underwater Views
  - WEC in Waves
  - Pitch Decay Test
  - WEC in Survival Seastate

7.2 Numerical Results

7.2.1 BEM Meshing and Modeling

BEM modeling was completed with WAMIT in addition to Capytaine, and the results from the former were utilized in forthcoming simulation. The presence of interior free surface waves and the difficulty of obtaining solver convergence on the thin-shell geometry describing the outer cylinder motivated this decision. The mesh used in the WAMIT run is given in Figure 29 and the run configuration parameters are given in Table 10. All geometry, input, and output files have been provided to the TEAMER partner.

Table 10: WAMIT Configuration

Number of CPU	3
RAM Cap	25 GB
Number of Bodies	3
Water Depth	6 m
Frequency Vector	[0:0.1:20],∞ (rad/s)
No. Panel, outer cyl.	1056
No. Panel, stabilizer	2407
No. Panel, water column	1169

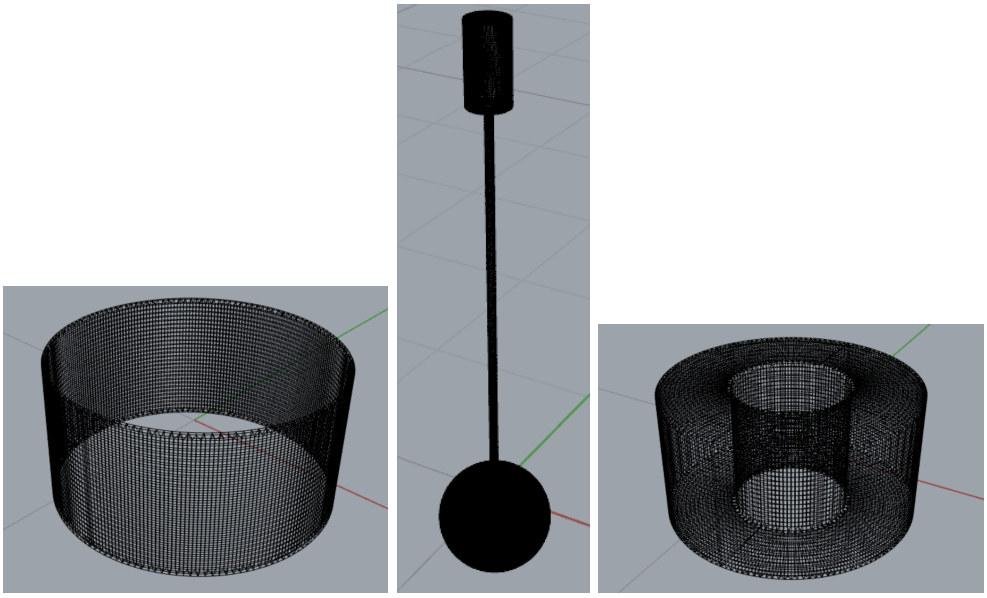

Figure 29: The *.gdf meshes used by WAMIT. From left to right, the outer cylinder, the stabilizer, and the contained water column, are shown. Note that the mesh only models up to the free surface, and that scale is not preserved between each sub-figure.

The hydrodynamic coefficients are shown in Figures 30, 31, and 32. While of sufficient quality for accurate simulation in WEC-Sim, there are some undesirable features of these coefficients that suggest future methodological improvements for the BEM analysis of OWC type devices. Firstly, in surge, the added mass terms ($A(\omega)$) do not converge to a constant at high frequencies. Secondly, radiation damping coefficients ($B(\omega)$) in pitch and surge do not converge to zero for all bodies. Both of these observations apply to the thin outer cylinder body: it is likely that the combination of the moonpool and the thin geometry introduced difficulties for the BEM solver, as these features did not resolve at higher mesh resolutions.

7.2.2 Initial WEC-Sim Modeling

The initial WEC-Sim model used a simplified translational PTO to couple the motion of the stabilizer and the contained water column. The motion is coupled by a spring-damper type PTO (Figure 33).

An enhanced version of this model was developed that used an idealized orifice model to couple the motion of the stabilizer and the water column (Figure 34). This model is the most similar to the device explored in laboratory-scale testing. However, both models are useful for two reasons. Firstly, the coupling forces introduced by an idealized orifice are well-approximated by a simple spring-damper. Secondly, the simple

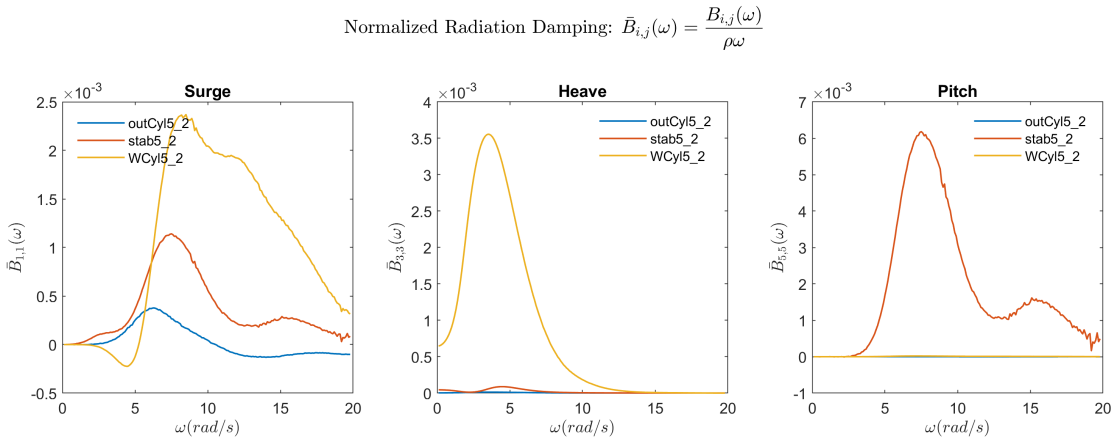

Notes:
• $\bar{B}_{i,j}(\omega)$ should tend towards zero within the specified ω range.
• Only $\bar{B}_{i,j}(\omega)$ for the surge, heave, and pitch DOFs are plotted here. If another DOF is significant to the system that $\bar{B}_{i,j}(\omega)$ should also be plotted and verified before proceeding.

Figure 30: The radiation damping coefficients estimated from the WAMIT boundary element method.

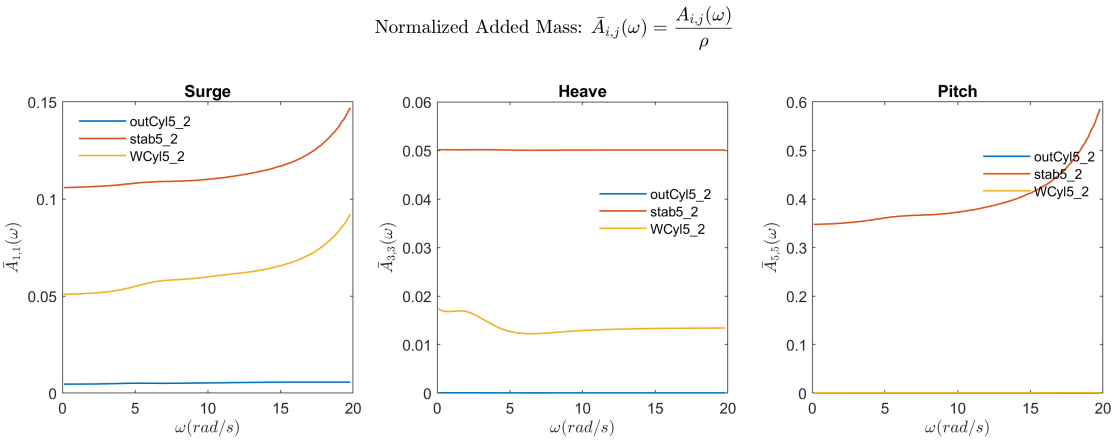

Notes:
• $\bar{A}_{i,j}(\omega)$ should tend towards a constant, A_∞, within the specified ω range.
• Only $\bar{A}_{i,j}(\omega)$ for the surge, heave, and pitch DOFs are plotted here. If another DOF is significant to the system, that $\bar{A}_{i,j}(\omega)$ should also be plotted and verified before proceeding.

Figure 31: The added mass coefficients estimated from the WAMIT boundary element method.

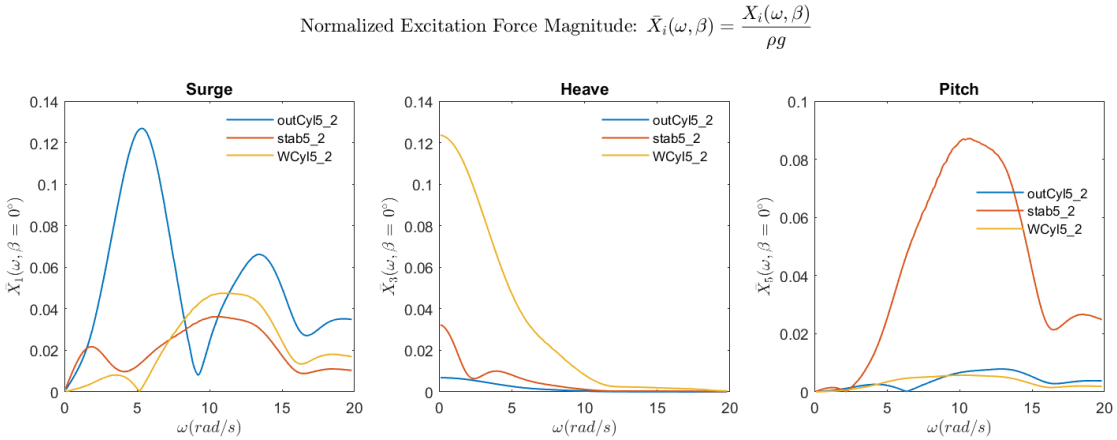

Figure 32: The excitation coefficients estimated from the WAMIT boundary element method.

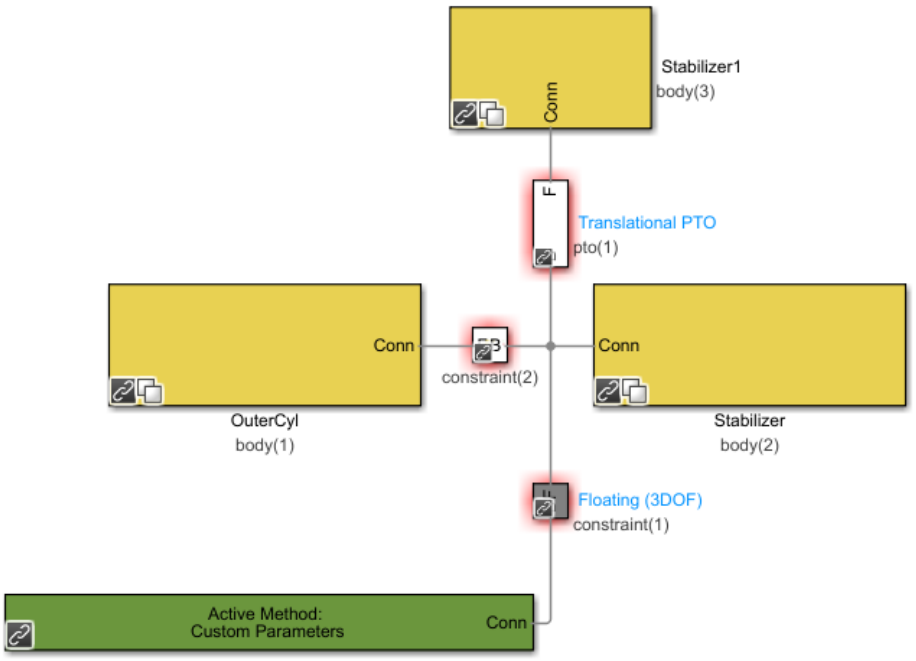

Figure 33: The WEC-Sim model using a simple power-take-off, used for system identification and control study.

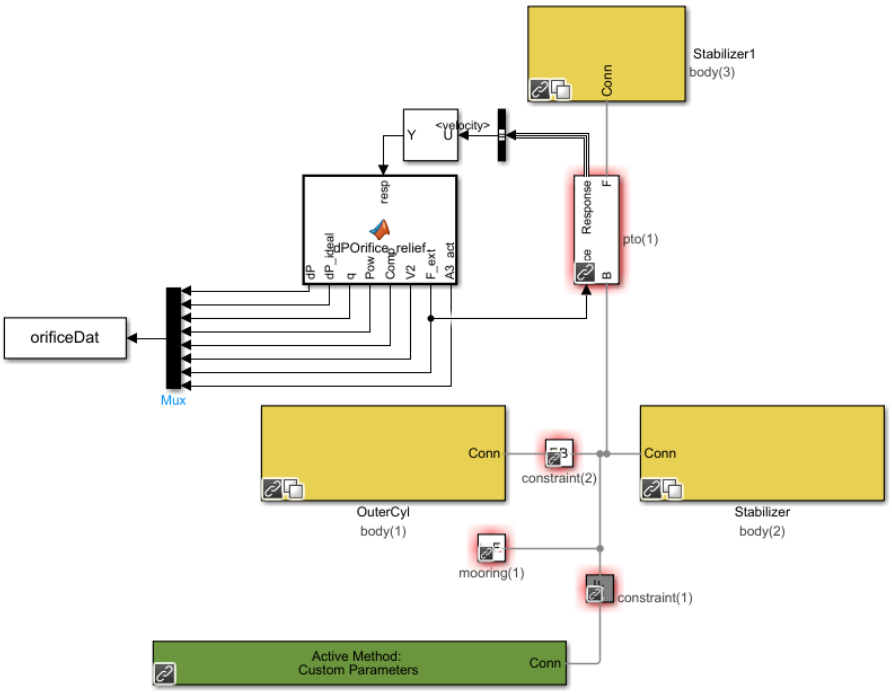

Figure 34: The WEC-Sim model using an idealized orifice, tuned to match laboratory experiments. The shown model includes the mooring model resulting from the tuning procedure.

translational PTO is more amenable to initial controls investigations.

7.2.3 System Identification and Control

In order to explore the potential gains associated with the application of a controller capable of delivering reactive power to the system, a linear model of the WEC admittance was derived by methods outlined in [1] by applying broad-band multisine forcing to the simplified PTO mode (Figure 35).

It is emphasized that these control results are not likely to be predictive of performance or system requirements, as they demonstrate potential mechanical power for an unconstrained system (Figure 36).
The feedback approximation of the complex-conjugate controller is more realistic than the complex conjugate controller in that it does not rely on perfect prediction of future excitation states, but remains highly optimistic (Figure 37).

Previous work has found that control settings that optimize mechanical power do not optimize electrical power capture (the actual figure of merit), and that it is critical to coordinate design of the PTO system, WEC, and

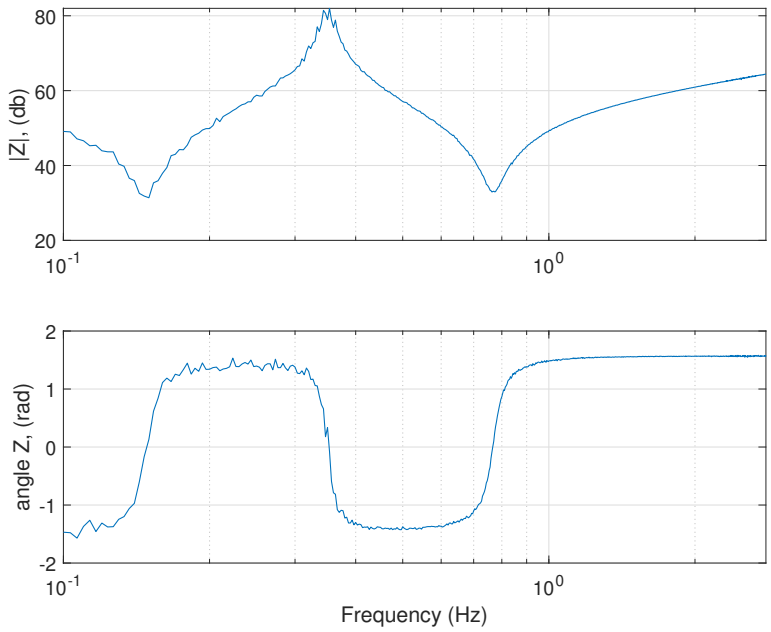

Figure 35: The identified impedance model Z of the relative motion between the stabilizer and contained water cylinder

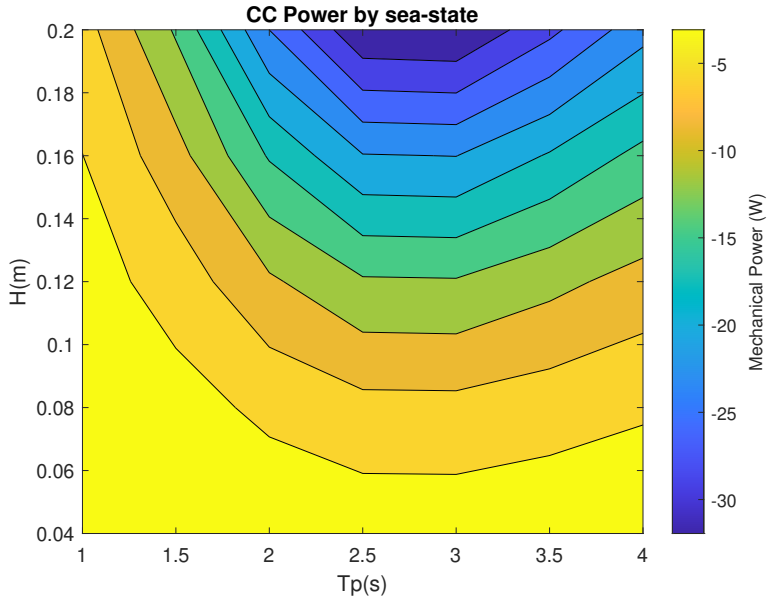

Figure 36: Mechanical power captured by a complex conjugate controller estimated from the linear impedance model. By sign convention, power capture is negative.

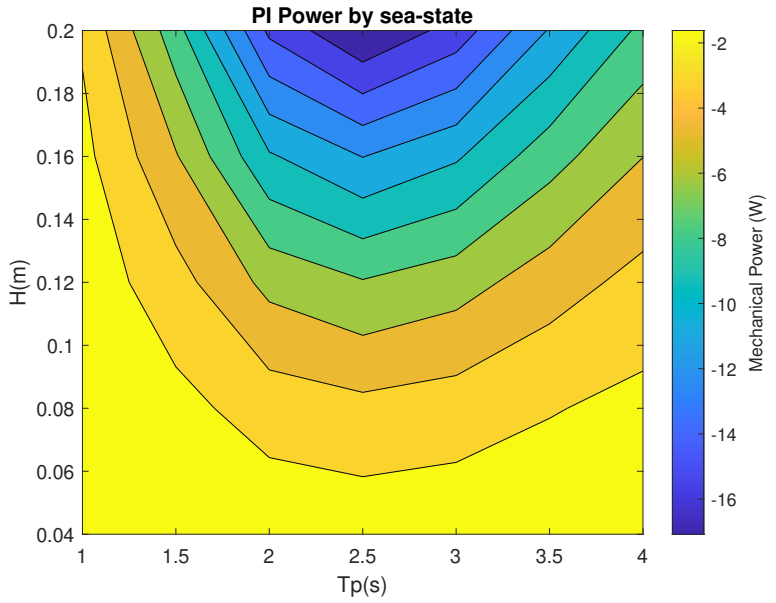

Figure 37: Mechanical power captured by a causal two-term PI controller approximation of a complex conjugate controller, estimated from the linear impedance model. By sign convention, power capture is negative.

control law to maximize electrical power for a realistic PTO [2].

As an example of this principle, an example is shown here in which a simple direct-drive mechanical-to-electrical converting PTO is considered with a winding resistance of 0.1 Ohm and a torque constant of 4 N-m/A. Note that we do not presume any specific physical architecture of the PTO: it is representative of the broad variety of systems that can be abstracted in this way mathematically. There is a significant reduction in available power, even with the minimal resistance applied at the generator. The sea-state with the largest available power has also changed: the addition of a PTO has substantially changed the resonant properties of the system (Figure 38). Note that the conclusions presented here have been found to apply generally to realistic PTOs (i.e., the specific parameters here were selected merely as an example) [2].

7.2.4 Model Tuning

The idealized orifice model was tuned to experimental results, beginning with an examination of free-decay response in heave. The heave decay procedure carried out in the lab is distinct from that conventionally utilized for model tuning. The model was thrust vertically downwards by a technician using a long pole. Thus, when the model is at its initial displacement

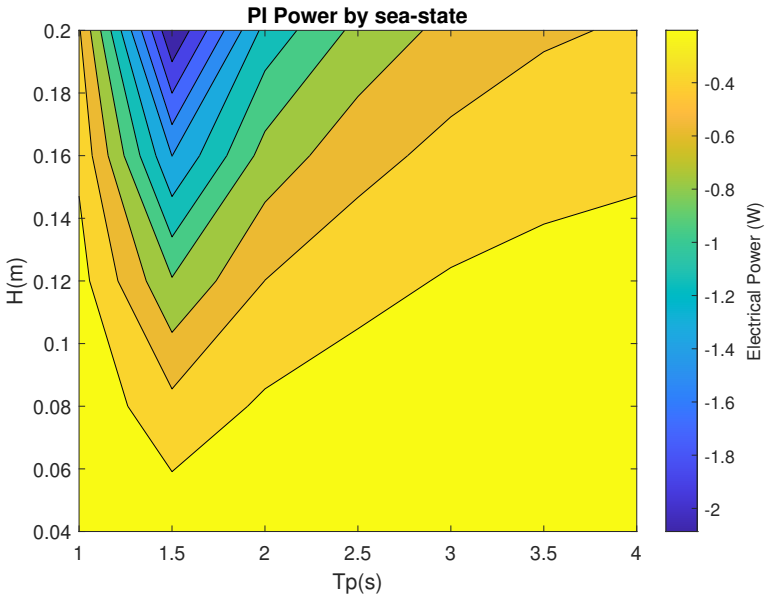

Figure 38: Electrical power captured by a causal two-term PI controller approximation of a complex conjugate controller, estimated from the linear impedance model. By sign convention, power capture is negative.

extrema, it is not wholly at rest, as it would be in the conventional procedure, and the conditions during the excitation are not known (there was no load cell in the pole used for actuation). Although it is possible to determine positions and velocities of each body from the recorded data, WEC-Sim solvers require that the body start from rest (i.e., there can be an initial displacement specified, but not an initial velocity). The initial conditions selected for model tuning are therefore determined at the first zero-crossing of the pressure drop across the orifice. At this point, no force is exerted between the two coupled bodies. Zeros of velocity were also considered, but the zeros of stabilizer velocity do not occur at the same instants as water cylinder velocity. Perfect quantitative agreement is not expected, since we are not including initial velocities, but decay frequencies and features are reproduced closely by the tuned model (Figures 39, 40, and 41. In particular, there are two unique features of the experimental data that are of interest and well-replicated by the model. Firstly, for both water level and heave position, the oscillation reverses direction prior to a zero-crossing. This is a hallmark of a 2-DOF oscillator with distinct resonant frequencies in each DOF, particularly when one DOF is subjected to larger damping forces. Secondly, these two resonant frequencies can be seen in the decay traces. In initial high-amplitude motion,

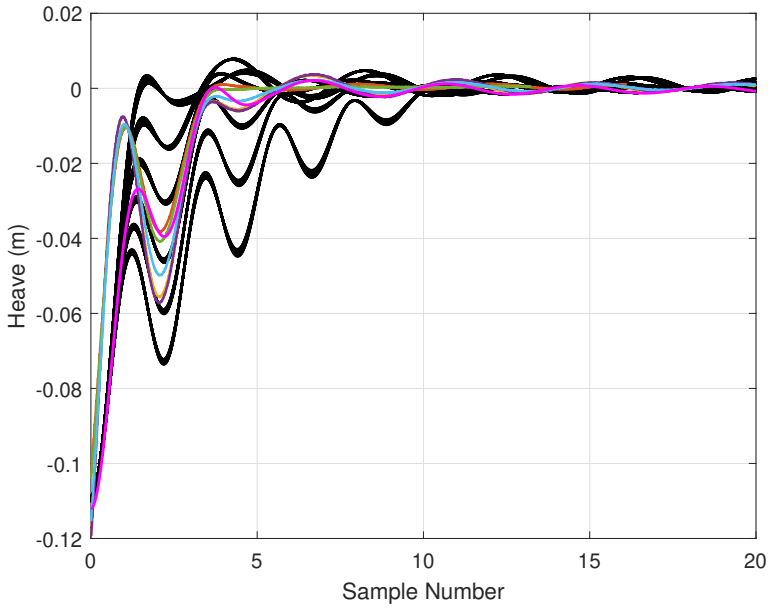

Figure 39: Model tuning of heave decay position for the large orifice. Laboratory results are shown as the colored lines (except magenta), tuning runs (N=288) are shown in black, and the selected tuning is shown as magenta.

where there is significant relative oscillation between the contained water column and the stabilizer, the dominant period is ~ 2.2 seconds. In later, lower-amplitude oscillation, where there is primarily solid-body motion of both the stabilizer and the contained water column, the dominant period is ~ 4 seconds. Similar conclusions hold for tuning of the small orifice model, with one additional remark: as noted by OTRC, water absorption over time decreased the still-water position of the model by about 2 cm: water absorption was not included in the WEC-Sim model, resulting in a difference in equilibrium position.

The parameter of most dynamic significance for the free-decay tests was the effective orifice diameter. Initially an ideal orifice, the effects of viscosity and any resulting *vena contracta* were not included. A correction term F adjusting orifice area was introduced as

$$A_2 = \pi(\frac{DF}{2}) \tag{2}$$

where A_2 is the effective area (m^2) of the orifice and D is the nominal orifice diameter. An effective orifice diameter is recommended for each of the small and large orifices from these results. However, because the physical mechanism of *vena contracta* formation is the viscous boundary layer near the orifice edges, the effective orifice diameter at any given in-

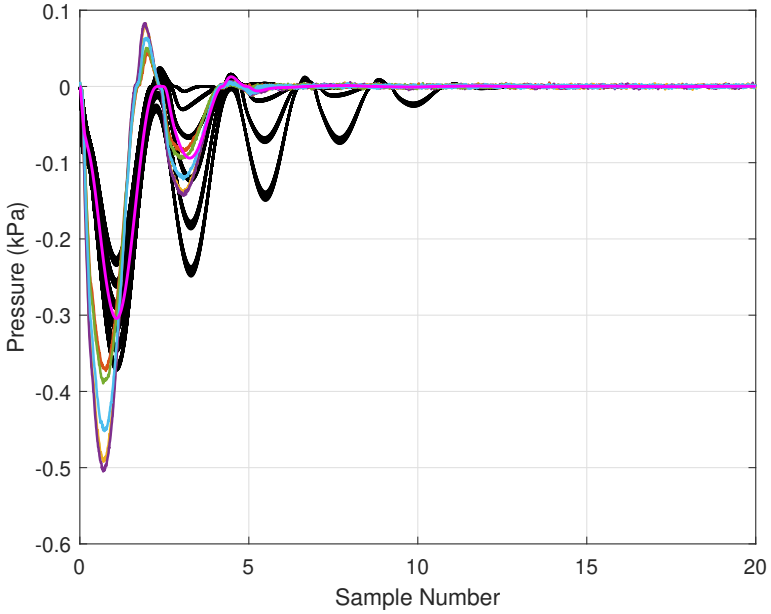

Figure 40: Model tuning of heave decay pressure for the large orifice. Laboratory results are shown as the colored lines (except magenta), tuning runs (N=288) are shown in black, and the selected tuning is shown as magenta.

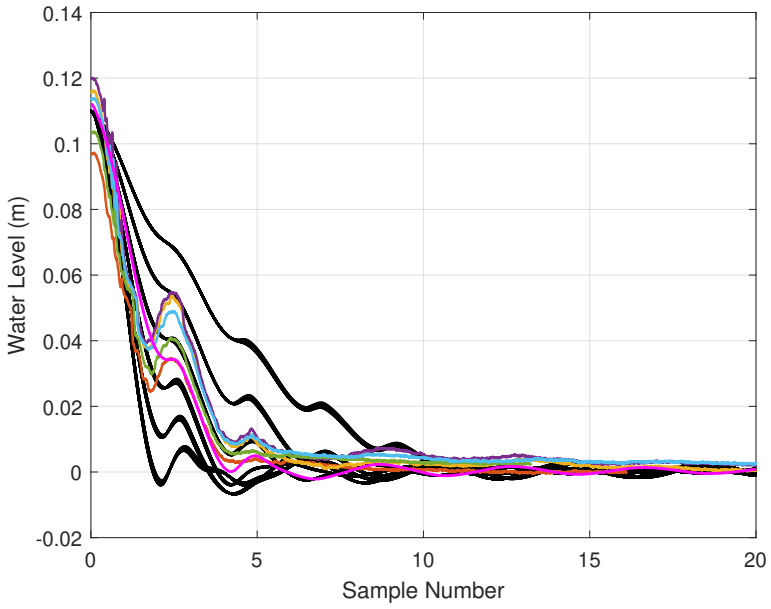

Figure 41: Model tuning of heave decay water level for the large orifice. Laboratory results are shown as the colored lines (except magenta), tuning runs (N=288) are shown in black, and the selected tuning is shown as magenta.

Table 11: Tuning parameters and selection

Parameter	**Value(s)**
F	[0.5:0.1]
C_d, stabilizer heave	[0.1:0.2:1.5]
C_d, water cyl. heave	[0.1:0.1:0.5]
F, selected	0.75
C_d stabilizer, selected	1.5
C_d water cyl. selected	0.1

Table 12: Mooring matrix stiffness estimated from surge offset tests

Displacement (m)	Stiffness (N/m)
< 0.75	11.24
> 0.75	118.62

stant depends upon flow velocity (i.e., the local Reynolds number) and the proposed diameters are suggested only as useful constant approximations. During tuning, this was tested at 6 different values, accounting for the 6 distinct black traces in Figures 39, 40, and 41. Other tuning parameters have a smaller effect: though shown, they are individually indistinguishable in these figures, and are summarized in Table 11. This procedure was repeated for both orifice diameters, and tuning selections were based on the results of both.

Surge static offset tests were conducted to determine the relationship between surge displacement and mooring stiffness. The mooring is a single-point catenary (Figure 5), and so the non-linear relationship is to be expected. It is well-approximated by two linear fits that depend on the magnitude of surge displacement (Figure 42). WEC-Sim uses a spring-damper matrix model to approximate moorings. A mooring matrix was added to the tuned simulation with a stiffness informed by laboratory static offset tests, noting that the median surge displacement in all wave cases is less than 0.5 m, well within the region for which the lower surge mooring stiffness was found to be appropriate (Table 12).

Because this is not the desired mooring configuration for a field-deployed device, the accuracy of the scheduled linear approximation, the minimal effect of the mooring on power capture, and the OTRC-provided ORCAFlex model of this test configuration, a MoorDyn model of this configuration was not pursued.

Further, the cross-correlation between the signals of each of the orthogonally mounted water level sensors was inspected for each wave case. An

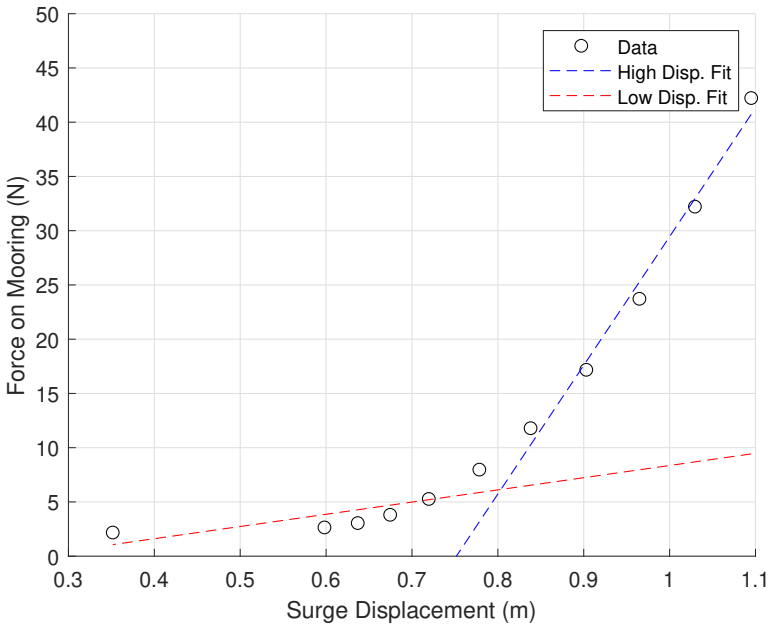

Figure 42: Linear fits of surge offset data used for model tuning.

example is shown in Figure 43 for the irregular wave run generating the largest power. In all cases, the signals demonstrate the strongest correlation at zero lag (and in the case of regular waves, integer multiples of the wave period), indicating that there are no "sloshing" modes induced by periodic stabilizer pitch motion. Further, in all except the survival wave state, the maximum pitch displacement observed was less than 5^o. This suggests that modeling the water cylinder-to-stabilizer coupling as a single degree of freedom translational constraint is sufficient.

For each orifice size and wave height, plots comparing laboratory and predicted average power capture for regular and irregular waves are shown in Figure 44 through 47. For regular waves, predictions are poor near resonance ($\sim$ 2 s), and more accurate at other frequencies. In narrow-banded (e.g. regular) waves, inaccuracy near resonance is a known shortcoming of boundary-element method analysis, and it is likely estimation errors in excitation and radiation coefficients near resonance propagate in simulation. In contrast, irregular wave predictions are accurate near resonance, but degrade in quality in the high-frequency sea-state, underestimating power capture for both orifice sizes.

More accurate tuning on a per-frequency or wave-type basis are possible by varying drag coefficients. It was also found that varying effective orifice diameter by modifying F to correspond exactly to the predomi-

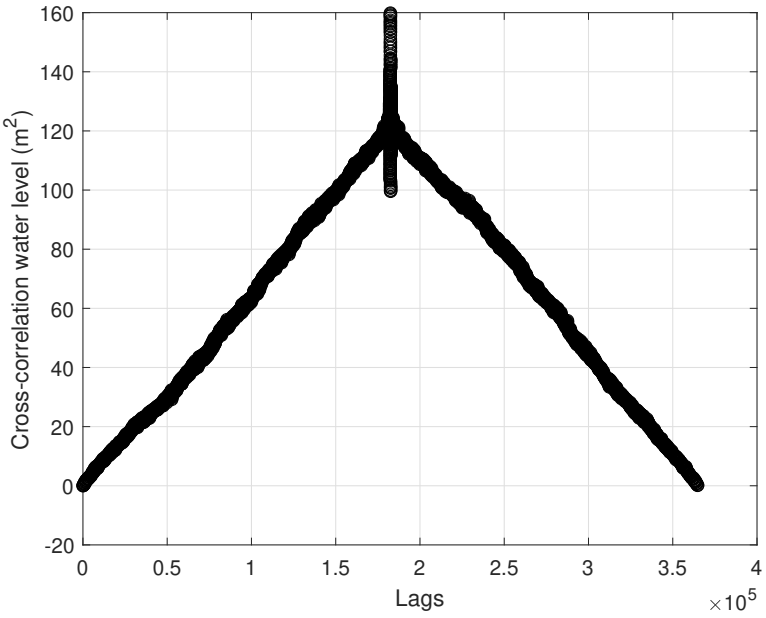

Figure 43: Cross-correlation between the two water level sensors.

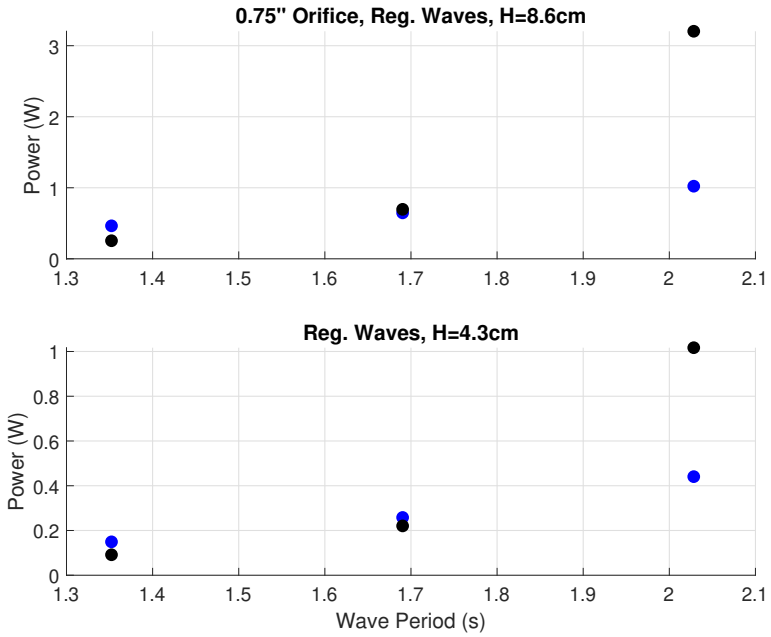

Figure 44: Comparison of power for the small orifice case in regular waves. The black dots indicate simulated results, and the blue are the laboratory results. This colormap is consistent through all similar plots.

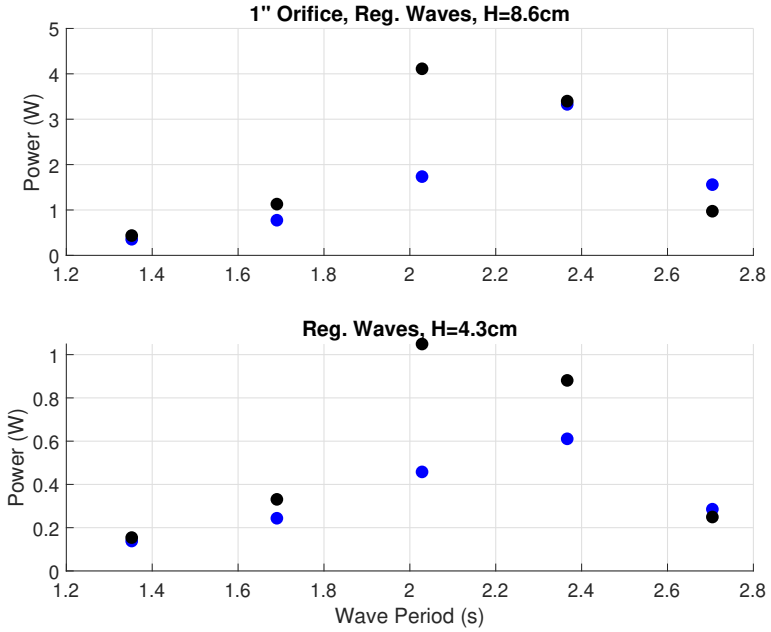

Figure 45: Comparison of power for the large orifice case in regular waves.

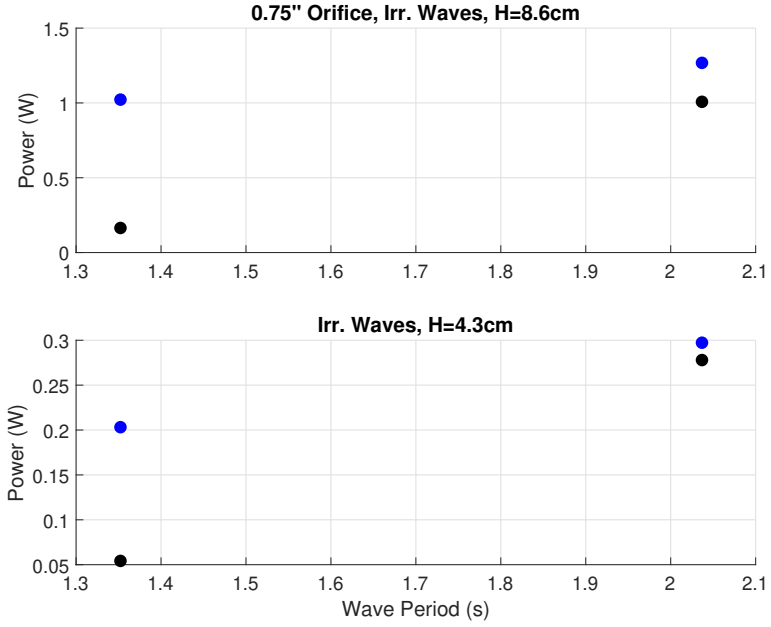

Figure 46: Comparison of power for the small orifice case in irregular waves.

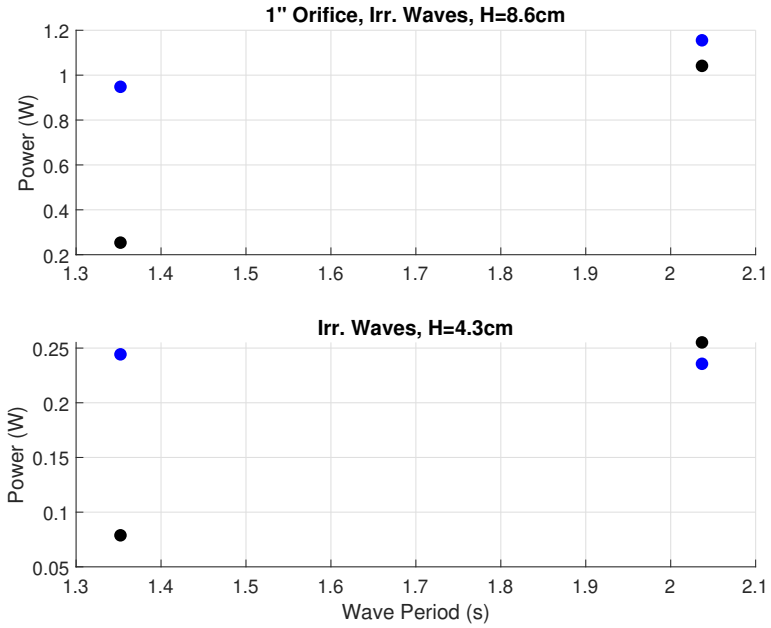

Figure 47: Comparison of power for the large orifice case in regular waves.

nant oscillating flow conditions at a particular sea-state can significantly reduce error. These methods are recommended if a particular sea-state is of interest. However, both of these methods tended to increase error at other conditions.

A relief valve on the orifice with a user-selected cracking pressure has also been implemented and tested to facilitate further work. However, because this feature did not exist in the laboratory tests it is not examined further here. In fact, the model used for tuning does include the orifice relief valve, but the cracking pressure is set arbitrarily high such that it never actuates.

7.2.5 Power and Load Surfaces

The tuned model was run over a grid of sea states for the large orifice size which has been found to consistently produce more power. These surfaces are presented in this section. Note that they may differ from surfaces provided for the EWTEC presentation, since these reflect the performance of the tuned model.

For irregular waves, which can exhibit run-to-run variability based on wave phase, the shown amplitude is calculated as a range between the 5th and 95th percentile (Figures 48 through 48). Regular waves, which do not depend on wave phase, are the full observed ranges.

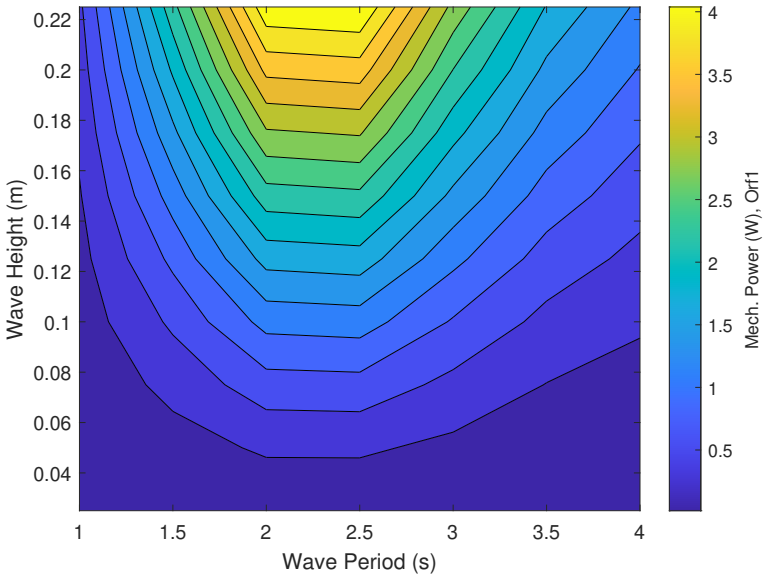

Figure 48: Modeled mechanical power surface for the tuned model in irregular waves.

The investigated WEC shows the best power capture under purely-resistive control (i.e., damping) across a fairly broad range of wave periods (1.7 to 2.7 seconds) owing to the selection of stabilizer and water column resonant frequencies resulting in two-body relative motion. This is particularly pronounced in irregular seas.

Even at the 1/35 scale model, orifice flow velocities in excess of 35 m/s are observed in irregular waves, and in excess of 45 m/s in regular waves. This suggests that in a larger-scale device, compressibility effects will be non-negligible. In addition to losses and potential thermal issues, this may complicate PTO design, particularly the design of a rotor that can efficiently extract energy from the both the incompressible and compressible flow regimes.

Further, loads exerted on the narrow spar connecting the outer cylinder structure to the stabilizer are likely to be significant. In heave, these loads exceed 22 N for the irregular waves, and 45 N in regular waves, and in surge 16 and 12 N, respectively. While it is noted that surge loads and heave loads are not maximized in the same sea-state, suggesting that a typical operating combined-loading case will be more modest than the superposition of the two individual maxima, a robust structural member is recommended, especially since the device does not incorporate any additional survival strategy.

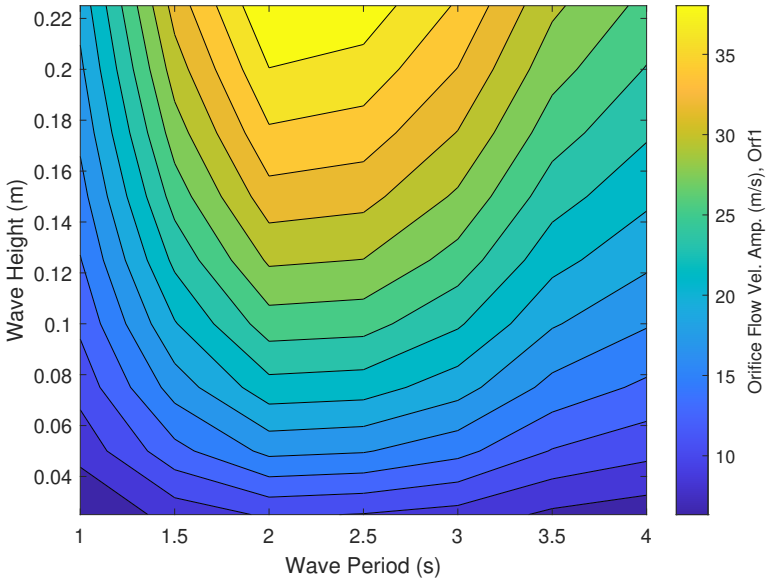

Figure 49: Modeled orifice velocity surface for the tuned model in irregular waves.

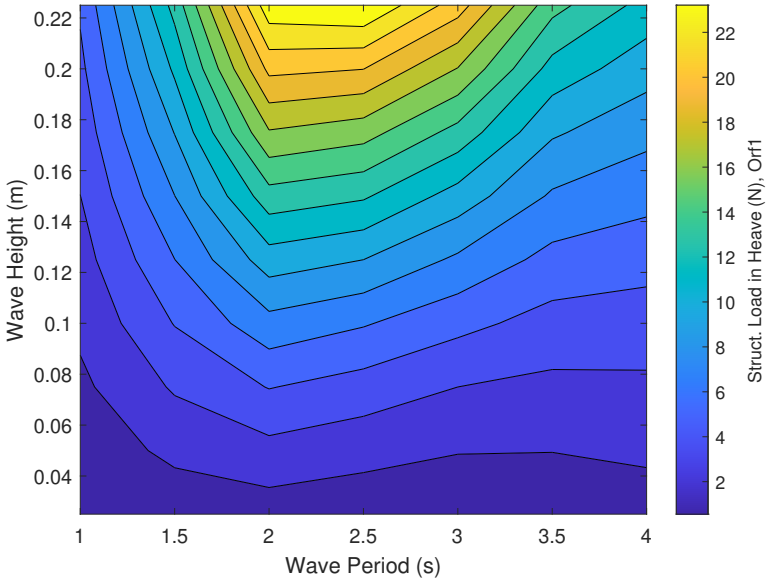

Figure 50: Modeled heave load surface for the tuned model in irregular waves.

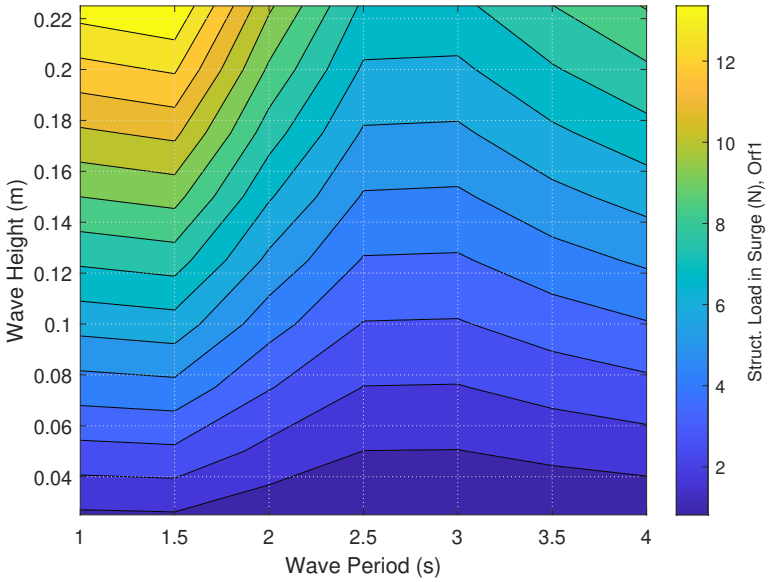

Figure 51: Modeled surge load surface for the tuned model in irregular waves.

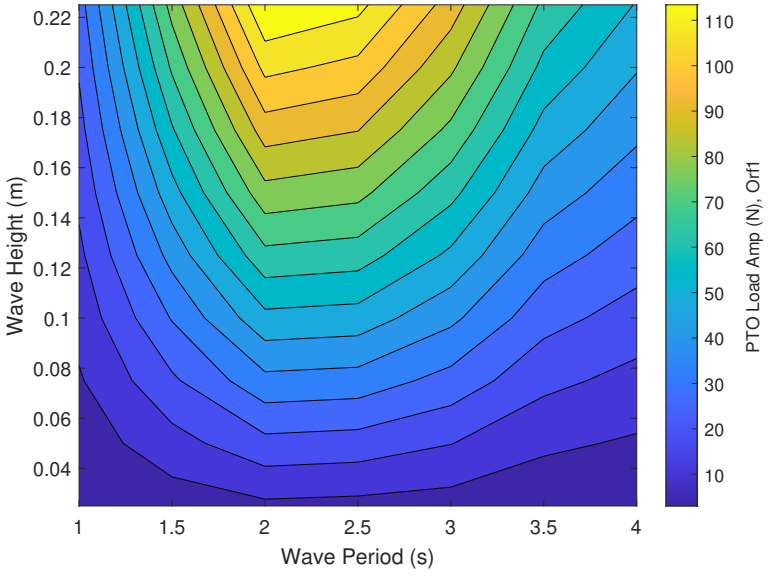

Figure 52: Modeled PTO load surface for the tuned model in irregular waves.

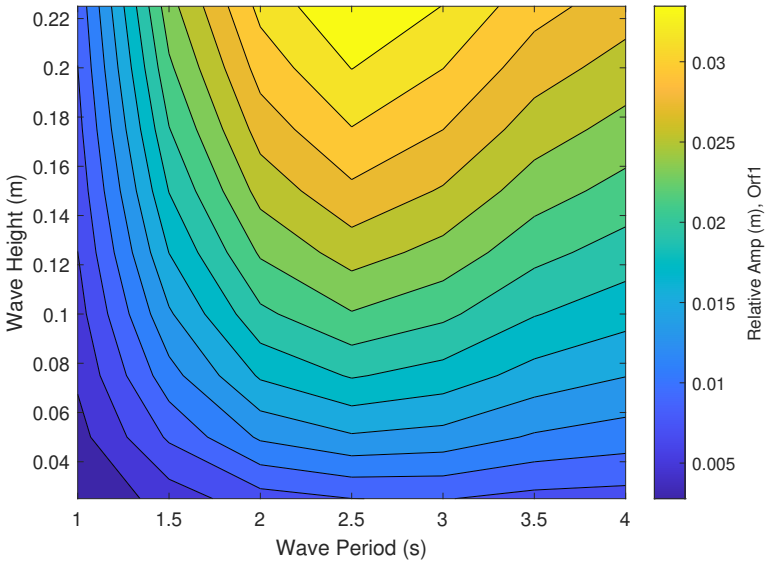

Figure 53: Modeled relative amplitude surface for the tuned model in irregular waves.

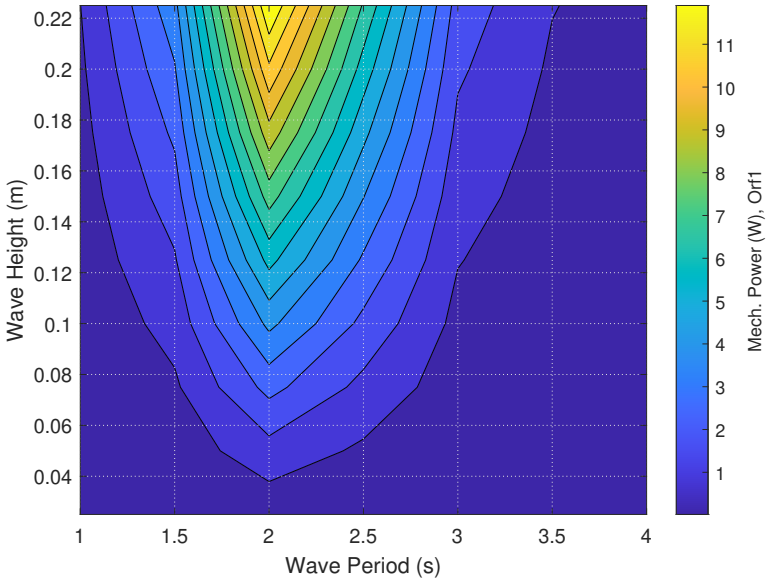

Figure 54: Modeled mechanical power surface for the tuned model in regular waves.

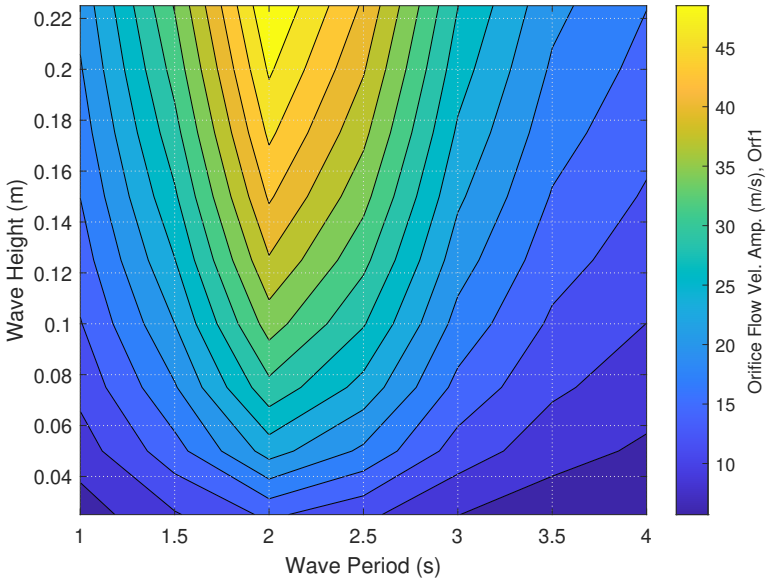

Figure 55: Modeled orifice velocity surface for the tuned model in regular waves.

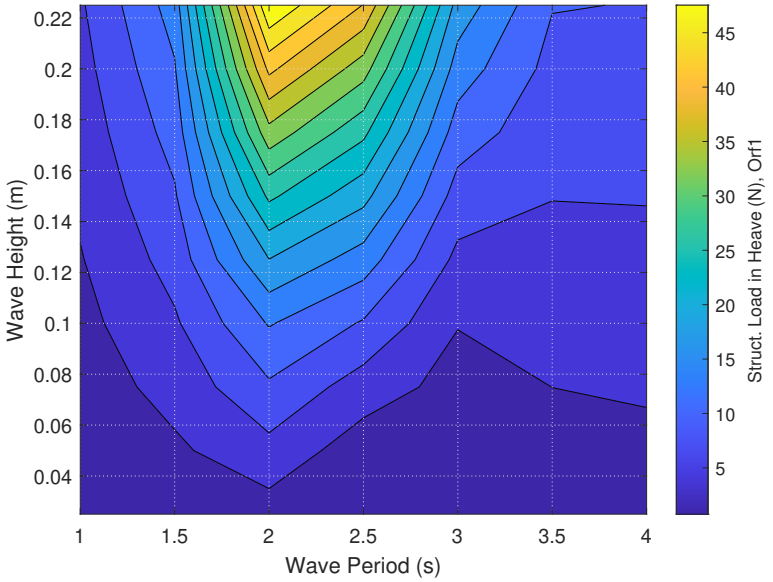

Figure 56: Modeled heave load surface for the tuned model in regular waves.

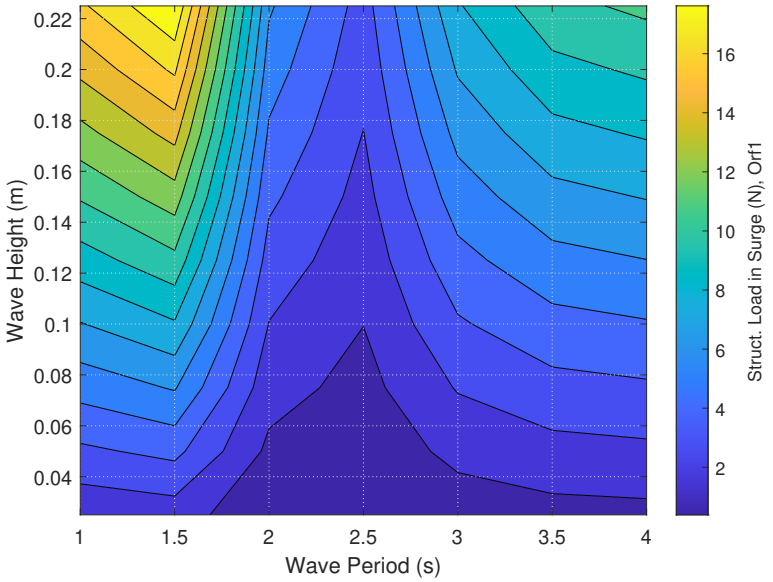

Figure 57: Modeled surge load surface for the tuned model in regular waves.

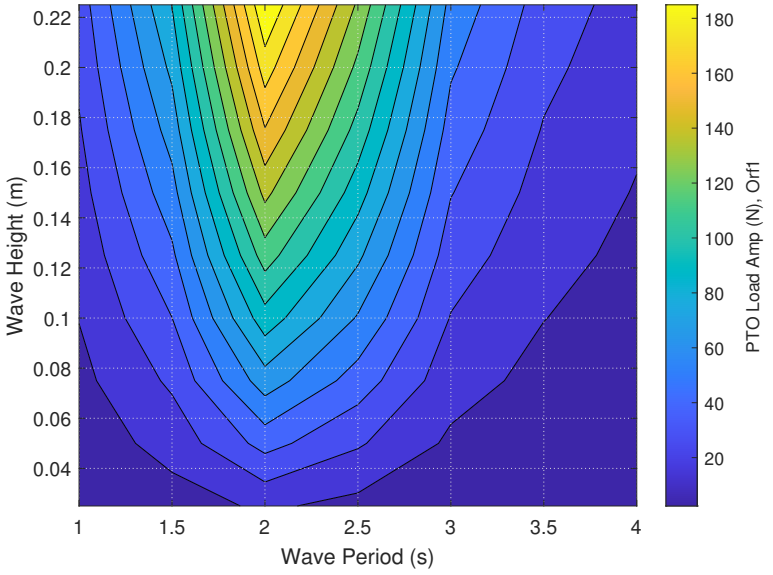

Figure 58: Modeled PTO load surface for the tuned model in regular waves.

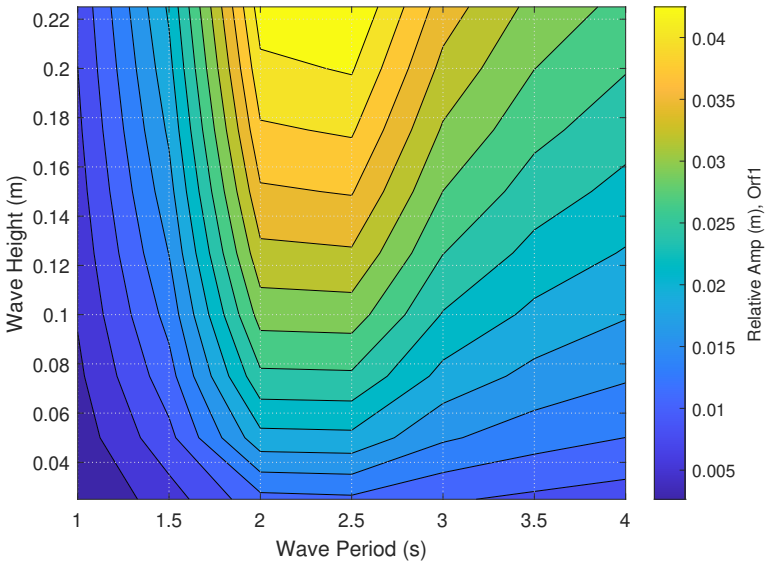

Figure 59: Modeled relative amplitude surface for the tuned model in regular waves.

8 Conclusions and Recommendations

The HiSeas device was successfully modeled using WEC-Sim with hydrodynamics informed from a WAMIT run following the OWC modeling suggestions of [3]. Heave decay comparisons indicate that the model captures key unique features of the WEC motion, and good agreement was generally found between laboratory and simulation power estimates for regular waves, while irregular waves, particularly those at higher frequencies, showed consistently larger error. A single set of tuning parameters informed from primarily from heave free-decay tests are recommended that are appropriate for most runs within the tested configurations: however it was found that run-specific tuning, specifically adjusting the F parameter describing effective orifice area, could reduce simulation error for the targeted case. Physically, this is intuitive: orifice pressures are unlikely to be accurately modeled with a single F across all sea states.

Because the WEC geometry is axisymmetric, it is likely ammenable to higher-order solution methods to BEM equations like those employed in WAMIT. In WAMIT, this requires modifying and re-compiling the FORTRAN-based geometric patch definitions. It is probable such an approach could improve BEM results and power capture estimates in irregular seas.

A 1-DOF linear impedance model of WEC admittance was developed for relative body motion to study potential controllers. This allowed an

idealized complex-conjugate controller to be examined in the frequency domain, along with the causal two-term complex-conjugate approximation of the form studied in [4] for the capture of mechanical power. It is noted throughout that this is not predictive of actual device performance, but does form a useful framework from which mechanical-to-electrical PTOs can be further studied. A simple example of the effect that such a PTO has on the resonant properties and electrical power capture efficiency of the system was provided to emphasize the importance of co-design of the WEC, controller, and meaningful simplifications of the PTO system to obtain efficient power capture. The controller optimization code appropriate for both mechanical or electrical power maximization has been provided.

The investigated WEC shows good power capture under purely-resistive control (i.e., damping) across a fairly broad range of wave periods (10 to 15 seconds, full-scale) owing to the selection of stabilizer and water column resonant frequencies resulting in two-body relative motion. That this is achieved with a static geometry should not be understated: these are promising characteristics. The next development steps include the development of a detailed model of an appropriate PTO and the eventual construction of a coupled WEC + PTO model. An air turbine, particularly one capable of efficiently delivering reactive power, will need to be designed in coordination with the WEC geometry: this is a key challenge that will push the state-of-the-art and industry forward.

Bibliography

[1] G. Bacelli, R. G. Coe, D. Patterson, and D. Wilson, "System identification of a heaving point absorber: Design of experiment and device modeling," *Energies*, vol. 10, no. 4, 2017.

[2] R. G. Coe, G. Bacelli, and D. Forbush, "A practical approach to wave energy modeling and control," *Renewable and Sustainable Energy Reviews*, vol. 142, no. December 2020, p. 110791, 2021. [Online]. Available: https://doi.org/10.1016/j.rser.2021.110791

[3] M. Penalba, T. Kelly, and J. V. Ringwood, "Using NEMOH for Modelling Wave Energy Converters : A Comparative Study with WAMIT," *12th European Wave and Tidal Energy Conference*, p. 10, 2017.

[4] D. D. Forbush, G. Bacelli, S. J. Spencer, and R. G. Coe,

"A self-tuning WEC controller for changing sea states," *IFAC-PapersOnLine*, vol. 53, no. 2, pp. 12 307–12 312, 2020. [Online]. Available: https://doi.org/10.1016/j.ifacol.2020.12.1185

9 Acknowledgements

Sandia National Laboratories is a multi-mission laboratory managed and operated by National Technology and Engineering Solutions of Sandia, LLC., a wholly owned subsidiary of Honeywell International, Inc., for the U.S. Department of Energy's National Nuclear Security Administration under contract DE-NA0003525. This paper describes objective technical results and analysis. Any subjective views or opinions that might be expressed in the paper do not necessarily represent the views of the U.S. Department of Energy or the United States Government.